

Applications of Shear-Induced Polarized Light Imaging (SIPLI) Technique for Mechano-Optical Rheology of Polymers and Soft Matter Materials

Oleksandr O. Mykhaylyk,¹ Nicholas J. Warren,¹ Andrew J. Parnell,² Gerhard Pfeifer,³ Joerg Laeuger⁴

¹Department of Chemistry, The University of Sheffield, Sheffield, S3 7HF, United Kingdom

²Department of Physics and Astronomy, The University of Sheffield, Sheffield, S3 7RH, United Kingdom

³Anton Paar GmbH, Anton-Paar-Strasse 20, 8054 Graz, Austria

⁴Anton Paar Germany GmbH, Helmuth-Hirth-Strasse 6, D-73760 Ostfildern, Germany

Correspondence to: O. O. Mykhaylyk (E-mail: o.mykhaylyk@sheffield.ac.uk)

Received 16 April 2016; accepted 31 May 2016; published online 18 June 2016

DOI: 10.1002/polb.24111

ABSTRACT: A new experimental method for studying the mechano-optical rheology of polymeric liquids and soft matter materials is presented. The method is based on a combination of rotational rheology and a recently developed optical technique—shear-induced polarized light imaging (SIPLI). The method provides a unique opportunity to monitor a complete sample view during rheological measurements in plate–plate and cone-and-plate geometry. Applications of the method are presented including simultaneous SIPLI and the rheology of the oriented lamellar phase of block copolymers and liquid crystals as well as a study of the thermally induced reversible

transformation of worm-like micelles to spherical micelles. In addition, a direct relation between the shish formation and the polymer melt viscosity upturn during flow-induced crystallization of semi-crystalline polymers is demonstrated. An application of SIPLI for quantitative birefringence measurements is also shown. © 2016 The Authors. Journal of Polymer Science Part B: Polymer Physics Published by Wiley Periodicals, Inc. *J. Polym. Sci., Part B: Polym. Phys.* **2016**, *54*, 2151–2170

KEYWORDS: birefringence; copolymers; liquid crystals; polymers; rheology; shear-induced polarized light imaging

INTRODUCTION Modern rheological instruments allow a wide range of methods to be used for testing the mechanical properties of soft matter materials and in particular, polymers. Among these instruments, rotational rheometers (stress-controlled and strain-controlled) are perhaps the most commonly used in academic and industrial research laboratories. This is mainly due to the fact that the rotational type devices allow facile variation of the shear-rate and/or shear-stress, and as such, it is possible to continuously shear a studied sample for a virtually unlimited period of time. This permits monitoring short-term transient behavior of the material as well as achieving a stationary state of flow in a single experiment. These experiments enable measurements of a number of rheological parameters, such as shear viscosity, normal stress, dynamic modulus and phase angle, yield stress, creep and stress relaxation.¹ The development of rotational rheometers during the last century² has resulted in these instruments being exploited not only for measurements in continuous and oscillatory shear using cone-and-plate, plate–plate or concentric cylinders (Couette or Searle approach) geometries, but also for dynamic mechanical anal-

ysis of materials in torsion and extension using torsion bar fixtures,³ and for extensional rheology of films using two counter rotating drums.⁴

There is a continuously growing interest in a combination of rotational rheology with other characterization techniques to perform simultaneous measurements of viscoelasticity and extra physical parameters associated with phase transitions, morphological transformations and structural orientation in soft matter materials. In recent decades, the versatility of rheology has been demonstrated by the progress of techniques such as rheo-infrared,⁵ rheo-Raman,⁶ rheo-optical microscopy, rheo-SALS (small-angle light scattering),^{7,8} rheo-SAXS (small-angle X-ray scattering),^{9–11} and rheo-SANS (small-angle neutron scattering).¹² The coupling of these techniques provides invaluable information about the relationship between macroscopic rheological properties and microscopic structural characteristics of materials. In this respect, particular attention has to be paid to rheo-birefringence measurements, where the collective behavior of macromolecules and nanoparticles can be detected via

© 2016 The Authors. Journal of Polymer Science Part B: Polymer Physics Published by Wiley Periodicals, Inc.

This is an open access article under the terms of the Creative Commons Attribution License, which permits use, distribution and reproduction in any medium, provided the original work is properly cited.

changes in the birefringence properties of a material. For example, birefringence occurs due to the flow-induced orientation of polymer chains or particles in polymer melts, solutions or particle suspensions which creates optical anisotropy. There was a strong period of activity in this field during the 60s and 70s of the last century (comprehensively described in two excellent books^{13,14}) including a number of fundamental mechano-optical rheological studies based on rotational shear geometries and flow birefringence.^{15,16}

The common feature of all these techniques used in combination with rotational rheology is that the data are collected from a small area of the sample which is defined by the cross section of the illuminating (optical techniques) or irradiating beam (SAXS or SANS). This approach is justifiable if assuming that the flow is laminar and the shear rate does not change significantly across the sample. It is therefore reasonable for the results obtained from a single point to be extrapolated over the whole sample and, consequently, complement the rheology data. Hence, this approach is mostly suitable for concentric cylinders and cone-and-plate geometries. However, this assumption is not always valid. For instance, in the case of shear banding when the secondary flow influences homogeneity of the sample flow. In addition, the point-like techniques fail when the shear flow across the sample is not constant as, for example, in plate-plate geometry. Therefore, it is always desirable to use a technique collecting information about different areas of the sample simultaneously and enabling large sample areas to be assessed during rheological measurements. In this respect, methods based on flow birefringence could be considered as suitable candidates. For example, flow birefringence has gained significant popularity as a way for direct visualization and measurements of fluid stresses in complex geometries,^{17,18} where relatively simple optical devices similar to a polariscope are used. Despite the fact that the flow field is well understood for rotational rheometers,¹⁹ flow visualization in these instruments may be essential for observations of the stress field associated with possible phase transitions and morphological transformations enhanced by the flow, when application of the constitutive equations of fluid mechanics are not valid.

It was recently shown that a reflection polariscope could be combined with a shearing device based on rotational plate-plate geometry. This instrument was used for the development of a new technique—shear-induced polarized light imaging (SIPLI).²⁰ The potential of the SIPLI technique has already been demonstrated by measurements of flow parameters for the onset of shear-induced crystallization in synthetic polymers and silk²¹ and by studying orientation of lamellar phase in diblock copolymer solutions.²² The key feature of the instrument is the dual functionality of the shearing plates, which act simultaneously as both the optical components of the reflection polariscope and the shearing tools. One of the plates, made of glass, is used as a window for viewing the sheared sample and the other plate, made of steel with a polished surface, is used as a mirror for reflecting light to obtain an image of the sample. The main advantage of this arrangement is that the polariscope occupies only

one side of the shearing device while the other side remains free. Such an arrangement of the optical components enables the reflection polariscope to be combined with a rotational rheometer. This assembly can provide a unique opportunity to carry out mechano-optical rheology, where mechanical measurements and optical observations of the stress field are performed simultaneously. Furthermore, the polariscope offers a chance to monitor, in full view, the sample online throughout the entire rheological experiment.

The main goal of this work is to describe basic theoretical and experimental principles of the SIPLI technique and to demonstrate potential applications of a rotational rheometer combined with a SIPLI device using mechano-optical rheological measurements of soft matter materials, in particular polymers. Herein, a number of case studies highlighting advantages of SIPLI technique are given, including a simple visualization of a material loaded in the rheometer, flow alignment of liquid crystals (LCs) and block copolymers, shear-induced crystallization of polymers, morphological transition of self-assembled block copolymer nanoparticles, and birefringence measurements of sheared polymer melts.

MATERIALS

A number of materials were chosen for this study to demonstrate the versatility of the SIPLI technique and the mechano-optical rheology method. Semi-crystalline polymers of industrial grade (LyondellBasell, Frankfurt am Main, Germany) such as high-density polyethylene, HDPE ($M_w = 227$ kDa, polydispersity $M_w/M_n = 14.5$ and nominal melting temperature $T_m = 133$ °C), and low-density polyethylene, LDPE (Lupolen 1840H, $M_w = 240$ kDa, $M_w/M_n = 14$ and $T_m = 112$ °C), were used for a flow-induced crystallization (FIC) study and birefringence measurements, respectively. 9 wt % A polystyrene–polyisoprene (PS–PI) diblock copolymer ($M_w = 1460$ kDa, $M_w/M_n = 1.04$, volume fractions of the blocks are 0.52 and 0.48, respectively) solution in a mixture of acrylate-based compounds²² and LCs (4'-octyl-4-biphenyl-carbonitrile, 8CB, Sigma-Aldrich, Gillingham, United Kingdom) were used for experiments on structural alignment. Finally, an aqueous dispersion of poly(glycerol monomethacrylate)₅₂-poly(2-hydroxypropyl methacrylate)₁₂₂ (PGMA₅₂-PHPMA₁₂₂) at 5 wt % solids²³ was used to demonstrate measurement of particle morphology transformations in colloidal systems.

EXPERIMENTAL SETUP

The optical setup for the SIPLI technique is based on the working principles of a reflection polariscope.²⁰ Hence, the mechano-optical rheometer proposed for simultaneous mechanical rheology and SIPLI measurements is combined of two main units: a rotational rheometer and a specially designed reflection polariscope attached to the rheometer (Fig. 1). The rheometer shearing disks perform a role of coupling components. The static disk, made of glass, is used as a viewing window and the rotating disk, made of stainless steel with a polished surface adjacent to the sample, is used

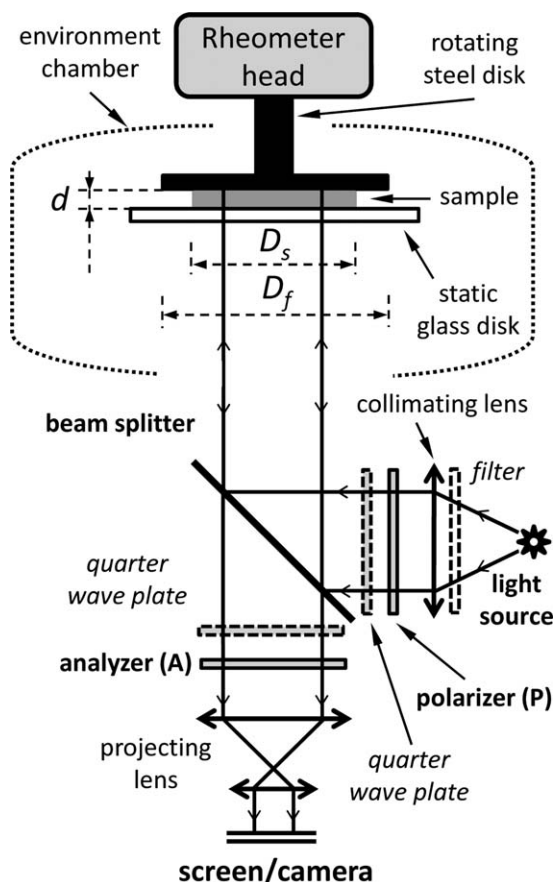


FIGURE 1 The optical setup of a mechano-optical rheometer for simultaneous mechanical rheology and SIPLI measurements. The main optical components of the setup are drawn in solid lines and assigned in bold. Supplementary optical components are drawn in dashed lines and assigned in italic. D_s , D_f , and d indicate the sheared sample diameter, the top (rotating) disk diameter and the sample thickness (the gap between the shearing surfaces of the rheometer), respectively.

as the mirror of the reflection polariscope. The mirror surface roughness is about $1 \mu\text{m}$ (obtained by fine polishing with a diamond paste) which is comparable with the wavelength of light but still significantly larger than the radius of gyration of polymer molecules. A reflection polariscope combined with the rheometer disks is called a SIPLI polariscope. Main components of the SIPLI polariscope are a light source, a linear polarizer, a beam splitter, a mirror (in this case the polished surface of the rotating disk), a linear analyzer, and a screen or camera. To perform quantitative birefringence measurements, a collimating lens, making the illuminating rays of the light source parallel, is incorporated in the optical system. The lens at the SIPLI polariscope exit projects a sample image onto a camera CCD chip (a Lumeana Lu165C color CCD camera was used for the measurements). The camera allows images, time-resolved frames or a video of a studied sample to be recorded during experiments. The components of the lower part of the SIPLI polariscope are coaxial with the rheometer axis of rotation. The polarizer and the analyzer are mounted on rotating holders

enabling an adjustment of mutual orientation of their polarization axes from parallel (0°) to orthogonal (90°). The instrument described in this work is equipped with a broadband light source (a halogen white lamp) connected to the optical components via a fiber optic cable. The whole spectrum of the source is used to illuminate a sample for obtaining polarized light images (PLIs) and monochromatized beam of the source (filtered by a drop-in narrow-band interference filter; Fig. 1) is used for birefringence measurements. However, a monochromatic light source such as a laser coupled with a beam expander could also be incorporated in this instrument for the sample illumination.

In the proposed optical setup one side of the sheared sample has to be accessible for viewing. In this respect, a Physica MCR rheometer (Anton Paar, Graz, Austria) equipped with a glass plate for optical applications (e.g., P-PTD 200/GL with a Peltier heating element or P-ETD 300/GL with an electrical heating element) is conveniently designed for the proposed mechano-optical rheometer. A slight modification of the glass plate has been to replace the original optical slit with an opening equal to the rotating disk diameter (D_f , Fig. 1) as this provides access to a full view of the sample surface. Moreover, there is enough space underneath the glass plate (including a heater) for mounting optical components of the SIPLI polariscope and allowing an unobstructed optical path between the light source and the sheared sample.

The optical path and the state of polarization of the light in the SIPLI polariscope can be described as follows. The parallel light rays collimated by the lens become plane-polarized after passing through the polarizer and the polarized light subsequently reflected off the beam splitter enters the rheometer sample region at 90° to the plane of shearing. Due to reflection from the rotating steel disk the rays make a double pass through both the static glass disk and the sample. The status of light polarization does not change when the light rays are reflected normally from a metal mirror. After exiting the rheometer, the light passes through the beam splitter, the analyzer and the projecting lens before finally reaching the camera (or a screen). For obtaining PLIs the mutual angle between polarization axes of the analyzer and the polarizer is usually set to 90° . If the sample is non-birefringent, the plane-polarized light illuminating the sample emerges from the rheometer with the same state of polarization as it entered the rheometer. As a consequence, the light with unaltered polarization is not transmitted through the analyzer, orthogonal to the axis of light polarization, and the sample appears dark in a PLI. Whereas, if the sample is birefringent, the orientation of the light polarization changes after passing through the rheometer. In this case the light will be transmitted through the analyzer, as the mutual orientation of axes of their polarization is likely to diverge from orthogonal, and a PLI containing information about birefringent properties of the sample is produced/imaged.

The standard heating elements supplied with the Physica MCR rheometer (e.g., an upper Peltier hood and a set of

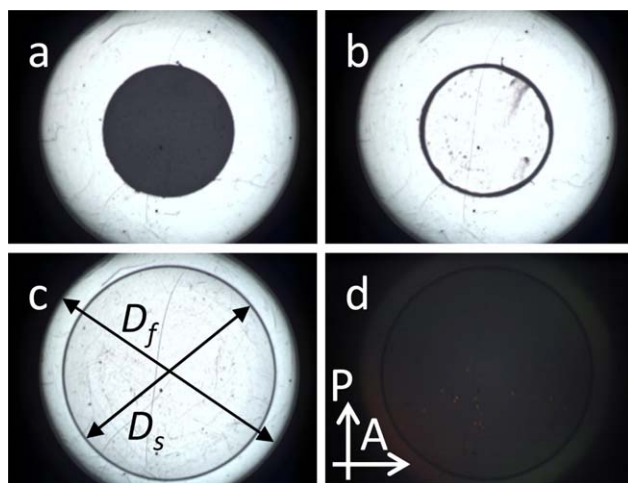


FIGURE 2 Images of a LDPE sample loaded onto the mechano-optical rheometer: (a) a solid sample disk (diameter $D_s = 12.5$ mm and sample thickness 2.3 mm) loaded at room temperature; the gap between the shearing plates of the rheometer, d , is set to 3 mm; (b) the same sample disk in a molten state at 125 °C; (c) the LDPE sample after setting the gap between the shearing disks [$d = 1$ mm, $D_s = 19$ mm, $D_f = 25$ mm and temperature 125 °C; D_s and D_f indicate the sample diameter and the rotating (top) disk diameter, respectively] and (d) the same sample as in (c) but the image is obtained with crossed polarizer and analyzer (their mutual orientation is shown by white arrows). The axes of polarization of the polarizer and the analyzer are set mutually parallel for the other images (a–c). [Color figure can be viewed in the online issue, which is available at wileyonlinelibrary.com.]

Peltier heaters underneath the static glass disks) are used for sample temperature control. For simplicity, these elements are shown in Figure 1 as an environment chamber. To avoid heating of the optics, the SIPLI polariscope is mounted on the instrument at a significant distance from the heating elements and separated from the rheometer by an insulating air gap enclosed between the glass shearing disk and an additional glass disk (not shown in Fig. 1) set under the shearing disk.

The SIPLI polariscope is designed in a way that the full surface of the rotating disk is illuminated, enabling the full shearing area of the sample to be visualized. This provides a number of extra benefits for both SIPLI and general rheological measurements. Setting the polarizer axis and the analyzer axis mutually parallel provides an optical view of the whole sample. This gives an additional control of the sample during loading, for example, aiding the sample to be placed centrally relative to the axis of rotation [Fig. 2(a)]. The full view of the sample also aids detection (and removal) of errant air bubbles that may become trapped during liquid sample loading and can significantly influence rheological measurements. Moreover, the sample state can be monitored online during thermal treatments [Fig. 2(b)]. The optical image also enables the sample dimensions to be controlled during the rheometer gap setting [Fig. 2(c)]. For example, the edge of a

polymer melt is clearly observed in the image and the sample diameter (D_s) can be easily measured. Since D_s is known, rheological measurements can be performed on a sample with a diameter smaller than the diameter of the shearing disk ($D_s < D_f$). This option provides a few advantages for the mechano-optical rheometer in a comparison with a standard rotational rheometer. When $D_s < D_f$, a trimming operation is excluded from the sample loading protocol. The sample diameter is not restricted by the shearing disk size and disks with a large diameter can be used for measurements on small sample quantities. This is especially important for biological studies when often the sample amount is limited. An additional benefit from the optical image option of the SIPLI polariscope is that a set of parallel plate fixtures with different diameters, usually required for a rheometer, becomes unnecessary as it can be replaced by one fixture of a large diameter. The points mentioned concerning aspects of sample loading, sample state monitoring and the sample diameter measurement can equally well be applied to rheological experiments using cone-and-plate geometry.

Access to the full view of a loaded sample enables a quick assessment of the sample stress to be undertaken before measurements. If the sample is non-birefringent (e.g., a relaxed unstressed polymer melt) setting axes of polarization of the polarizer and analyzer mutually orthogonal shuts the light and the sample appears black in the PLI [Fig. 2(d)]. Crossing the polarizer and analyzer before the rheometer gap setting also helps monitoring sample residual stress. It was found that during the gap setting a polymer melt PLI turns completely black (the sample becomes non-birefringent) only when the normal force value measured by the rheometer transducer is below 0.1 N.

THEORETICAL BACKGROUND

PLIs observed in a polariscope are defined by the birefringent properties of a studied material. Such properties can be represented by its optical indicatrix, whose imaginary surface is formed by the refractive indices corresponding to different propagating directions of light [Fig. 3(a)]. Commonly, viscoelastic liquids under quiescent conditions are optically isotropic, that is these materials have one refractive index for all directions which form a spherical indicatrix. However, under impact of shear (or extensional) flow, refractive indices of an isotropic viscoelastic liquid can become uniaxially anisotropic, resulting in ellipsoidal indicatrix associated with birefringence.¹⁴ This anisotropy arises from stretching, deformation and/or orientation of the molecules along the direction of flow. In this case, the optical indicatrix of the material transforms from a spherical shape to an ellipsoid with its semi-axes length proportional to the principal refractive indices. One of the principal refractive indices, n_o , is called ordinary refractive index and the other, n_e , is principle extraordinary refractive index [Fig. 3(a)]. For positive birefringence, where $n_o < n_e$, the optical indicatrix forms a prolate ellipsoid [Fig. 3(a)] whereas for negative birefringence, where $n_o > n_e$, the optical indicatrix is an oblate ellipsoid. If

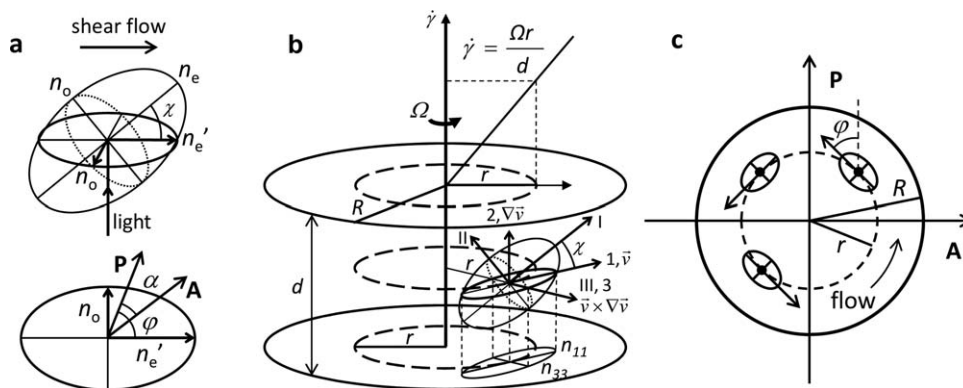


FIGURE 3 (a) An optical indicatrix of a sheared viscoelastic liquid (a prolate ellipsoid is taken as an example) with semi-axes corresponding to ordinary (n_o) and principal extraordinary (n_e) refractive index. The vectors assigned by **P** and **A** show polarizer and analyzer axis, respectively. (b) The optical indicatrix (coaxial with the stress ellipsoid) of a single point of a viscoelastic liquid sample disk [$2R = D_s$, see Fig. 2(c)], subjected to a shear in plate–plate geometry. Mutual orientations of the laboratory coordinate axes corresponding to velocity (1), velocity gradient (2), and neutral or vorticity (3) directions and the principal directions of stress (I, II, and III) at this point of the sample are shown. The light beam propagates along axis 2 (see Fig. 1 for a reference). χ is the angle of orientation of the stress ellipsoid [equivalent to the optical extinction angle, see eq 1 and section (a) of this figure]. A projection of the indicatrix section onto the shearing disk plane is shown, in accordance with (a) $n_{33} = n_o$ and $n_{11} = n_e$. A shear rate distribution across the sample, $\dot{\gamma}$, is shown at the top of the drawing, where d is the sample thickness, r is the radial position of the point, and Ω is the angular speed of rotation of the shearing disk. (c) A view of the sheared liquid sample from the top (the axis of rotation of the rheometer is normal to the figure plane) with the projections of indicatrix sections corresponding to sample points at a radial position r .

a light beam travels along the axis corresponding to n_e , the wave front coincides with the circular section of the optical indicatrix ellipsoid and no birefringence is observed, the light beam experiences n_o only. However, for a light beam propagating along all other directions, two refractive indices should be considered: one for the *ordinary* direction of electromagnetic vibration lying in the circular section of the indicatrix with refractive index n_o and another for the *extraordinary* direction of electromagnetic direction lying in the plane perpendicular to the light beam direction and perpendicular to the ordinary vibration direction with the refractive index n_e [Fig. 3(a)]. The n_e value can be obtained from n_o and n_e using equation:

$$\frac{(n'_e \cos \chi)^2}{n_o^2} + \frac{(n'_e \sin \chi)^2}{n_e^2} = 1 \quad (1)$$

where χ is the angle between the major axis of the ellipsoid and the major axis of the elliptical section.²⁴ When plane-polarized light enters a birefringent viscoelastic liquid, the light is broken up into two components (the ordinary ray and the extraordinary ray). Since these two components travel through the material with different velocities, a shift between phases of their electromagnetic waves arises and as a result the light after passing through the material changes its polarization to elliptical (for a general case), circular (if the phase shift is proportional to a quarter wavelength of the illuminating light), and linear (if the phase shift is proportional to a half wavelength of the illuminating light). The birefringent properties of viscoelastic liquids are often exploited for flow visualization^{17,19} or determination of the material stress parameters.¹⁴

If a viscoelastic liquid is subjected to a shear flow, a stress-induced birefringence arises. For the plane-polarized monochromatic light, used for the sample illumination in the proposed optical setup (Fig. 1), the phase shift between the ordinary ray and the extraordinary ray transmitted through the rheometer for each point of the sample surface can be expressed as:²⁴

$$\delta = \frac{2\pi}{\lambda} \Delta n 2d \quad (2)$$

where λ is the wavelength of light, d is the sample thickness (it is accounted for eq 2 that the beam passes twice through the material). The difference $\Delta n = n'_e - n_o$ quantifies birefringence of the material at the sample point. The term $\Delta n 2d$ is the optical retardation. It is assumed in eq 2 that only sample birefringence can contribute to the phase shift and that the other optical components of the system, such as the static glass disk (Fig. 1), are optically isotropic (i.e., they are non-birefringent) and that the polished metal surface of the rotating disk does not change the phase of electromagnetic waves upon reflection. If the sample is not subjected to a shear, that is the liquid remains in an isotropic state and non-birefringent ($\Delta n = 0$), no phase shift occurs under quiescent conditions, $\delta = 0$.

The image intensity at each point of a sample PLI produced by the interference of two monochromatic waves (i.e., the ordinary ray and the extraordinary ray) emerging from the rheometer with phase difference δ is given by:²⁴

$$I = I_o + I'_e + 2\sqrt{I_o I'_e} \cos \delta \quad (3)$$

where I_o and I'_e are the intensity of the two respective waves. It can be shown that the intensity of light passing through a

set of optical components such as linear polarizer—uniaxially birefringent (sheared) material—linear analyzer [Figs. 1 and 3(b)] can be expressed from eq 3, by using trigonometric relationships between the waves amplitudes, as:²⁴

$$I = I_s \left[\cos^2 \alpha - \sin 2\phi \sin 2(\phi - \alpha) \sin^2 \frac{\delta}{2} \right] \quad (4)$$

where α is the angle between the polarizer axis and the analyzer axis, ϕ is the angle between the polarizer axis and the ellipse semi-axis associated with the extraordinary refractive index n_e of the corresponding sample point and I_s is the intensity of light entering the system [Fig. 3(a), low part]. It has to be noted that only polarization-active components of the SIPLI polariscope are considered in eq 4. When the analyzer and the polarizer are set mutually orthogonal ($\alpha = \pi/2$) eq 4 reduces to:

$$I_{\perp} = I_s \sin^2 2\phi \sin^2 \frac{\delta}{2}. \quad (5)$$

If the mutual orientation of the polarizer axis and the optical indicatrix of the material at the corresponding sample point as such that $\phi = \pi/4$ a further simplification of eq 5 can be made:

$$I_{\perp} = I_s \sin^2 \frac{\delta}{2}. \quad (6)$$

Equation 6 corresponds to the conditions where the light emerging from the rheometer is at its maximum intensity. These conditions ($\alpha = \pi/2$ and $\phi = \pi/4$) are usually exploited in optical experiments for maximizing the sensitivity of birefringence measurements. Thus, if the intensities are measurable experimentally and the mutual orientations of the polarization-active components are known [Fig. 3(a)], δ can be obtained from eqs (4–6) and, consequently, the birefringence Δn can be calculated from eq 2 for each point of a PLI recorded during mechano-optical measurements. Alternatively, if the birefringence properties of a material and the mutual orientation of the components are known, a PLI of the sheared material can be predicted from eqs (4–6).

For practical reasons, the PLI of a sheared viscoelastic liquid, calculated for mutually perpendicular analyzer and polarizer (eqs 5 and 6), is used as an example. Stress is radially distributed in rotational plate–plate geometry. Thus, the stress (and associated birefringence) should be constant along the circumference of a particular radius. Assuming that the flow is laminar and that the direction of the shear flow corresponding to the same shear rate forms a circle, the orientation of optical indicatrices of the sheared material at each point of the sample is known *a priori* [Fig. 3(c)]. The major axis of the optical indicatrix projection ellipse is always tangential to the circle. Hence, angle ϕ between the polarizer axis and the ellipse semi-axis associated with the extraordinary refractive index ($n_{11} = n_e$) is already defined for each point of the sample. Thus, to calculate I_{\perp} from eq 5, only δ at each point of the sample disk has to be known. In this respect, it would be interesting to consider two cases for the

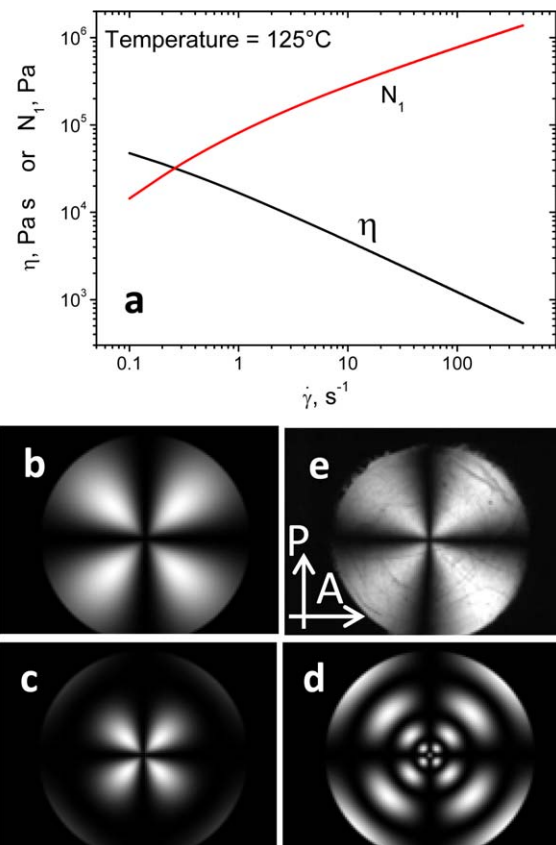


FIGURE 4 (a) The shear-rate dependence of both viscosity (η) and first normal stress difference (N_1) of a LDPE melt at temperature 125 °C. The viscosity is presented by a fitting curve to experimental data using Cross model, eq 10 ($\eta_0 = 128,538$ Pa s, $\dot{\gamma}_c = 0.04$ s⁻¹ and $m = 0.6$), and the N_1 curve is calculated using eqs 9 and 10. Calculated (b–d) and experimental (e) PLIs of the LDPE melt in SIPLI polariscope under a steady-state shear at 125 °C. The following parameters were used for the calculations and the experiment: wavelength of light $\lambda = 500$ nm, gap between the shearing plates $d = 0.7$ mm, radius of the sample $R = 12.5$ mm and angular speed $\Omega = 0.15$ rad/s (b), 0.3 rad/s (c), 6.0 rad/s (d), and 0.2 rad/s (e). In each image the shear rate changes radially across the sample from 0 rad/s (at the sample center) to $\dot{\gamma}_{\max} = \Omega R/d$ (at the sample edge), $\dot{\gamma}_{\max} = 2.68$ s⁻¹ (b), 5.36 s⁻¹ (c), 107.14 s⁻¹ (d), and 3.57 s⁻¹ (e). The polarizer (P) and analyzer (A) axes are set orthogonal (b–e). [Color figure can be viewed in the online issue, which is available at wileyonlinelibrary.com.]

radial distribution of δ : (i) when birefringence changes gradually along the sample radius (such as that observed in sheared polymer melts²⁰) (Fig. 4) and (ii) a stepwise change of birefringence along the radius of the sheared material (such as that observed for a diblock copolymer lamellar phase, where a sharp transition of the lamella orientation from perpendicular to parallel occurs at a particular shear rate²²) (Fig. 5).

Case (i) will be considered first, where the relative intensity of points of a sheared polymer melt using monochromatic

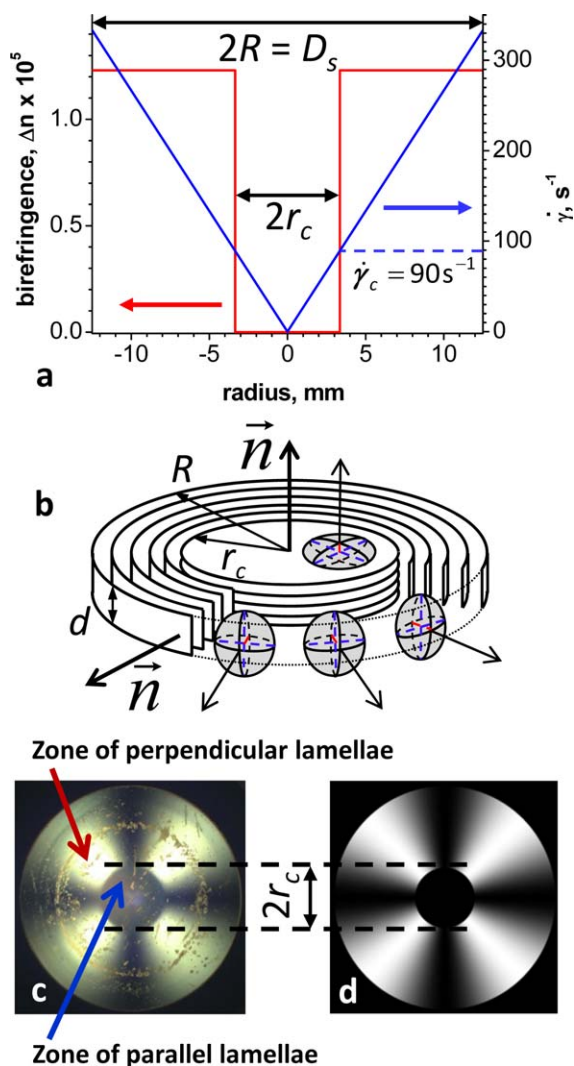


FIGURE 5 SIPLI observation of the parallel-to-perpendicular transition of lamella orientation for a 9 wt % polystyrene–polyisoprene (PS–PI) diblock copolymer in acrylate solution: (a) radial distribution of both shear rate (dashed blue line) and birefringence of the copolymer solution (solid red line) in rotational plate–plate geometry; (b) a schematic diagram of the lamella orientation together with the lamella optical indicatrices (oblate ellipsoids) in the sheared copolymer sample; (c) experimental and (d) calculated PLI of the PS–PI copolymer solution solidified by UV radiation after shearing (sample diameter $D_s = 2R = 25$ mm, angular speed of rotation $\Omega = 13.33$ rad/s and $d = 0.5$ mm), the axes of polarizer and analyzer are set orthogonal. [Color figure can be viewed in the online issue, which is available at wileyonlinelibrary.com.]

PLI can be described with the aid of eq 5. Corresponding points on the sample have a unique set of three orthogonal principal stress directions coaxial with the indicatrix ellipsoid axes [Fig. 3(b), basis vectors I, II, and III]. The neutral direction (vector III) is parallel to the radial direction of the point. For the stress measurements in rotational plate–plate geometry it is more convenient to use a laboratory Cartesian coordinate system [Fig. 3(b), basis vectors 1, 2, and 3]. The

vector 1 of the laboratory system is chosen to be parallel to the flow direction, the vector 2 is parallel to the velocity gradient direction, and the vector 3 is the neutral (vorticity) direction.¹⁴ The basis vectors of the laboratory coordinate system and the principal stress directions relate to each other as such that the vector 3 and the vector III are collinear and the vectors 1, 2, I, and II are coplanar (i.e., all four vectors lie in the same plane) [Fig. 3(b)]. The angle χ between the vector 1 and the vector I is referred as the extinction angle (or the orientation angle of the optical indicatrix). The ellipse projected onto the low shearing plate [Fig. 3(b)] represents a cross section of the sheared melt optical indicatrix by the 1,3-plane (the plane of PLI observations) which is perpendicular to the light beam. Thus, the 1,3-plane birefringence for each point of the sample can be expressed as

$$\Delta n_{1,3} = n_{11} - n_{33} = C(\sigma_{11} - \sigma_{33}) = 2C\sigma_{12} \cot 2\chi (h+1) \quad (7)$$

where C is the stress–optical coefficient (SOC) and $h = (\sigma_{22} - \sigma_{33}) / (\sigma_{11} - \sigma_{22})$.²⁵ σ_{ij} are components of the stress tensor associated with the laboratory coordinate system, where σ_{11} , σ_{22} , and σ_{33} are the normal stress components (the diagonal components of the tensor) at this point. In contrast to flow birefringence measurements in the 1,2-plane,²⁶ the 1,3-plane observations do not allow χ to be measured. However, considering the coaxiality of the stress ellipsoid and the indicatrix ellipsoid¹⁴ the cotangent of the optical extinction angle can be obtained from the recoverable shear $2 \cot 2\chi = (\sigma_{11} - \sigma_{22}) / \sigma_{12}$.²⁷ Thus, eq 7 can be rewritten as

$$\Delta n_{1,3} = C(\sigma_{11} - \sigma_{22})(h+1). \quad (8)$$

Since the second normal stress difference $N_2 = |\sigma_{22} - \sigma_{33}|$ is much smaller than the first normal stress difference $N_1 = |\sigma_{11} - \sigma_{22}|$,^{14,15,25,28} h is close to zero and can be neglected in eq 8. Thus, if both N_1 and SOC values are known, the birefringence of the polymer melt in the plane of PLI observations can be calculated from

$$\Delta n_{1,3} \approx C(\sigma_{11} - \sigma_{22}) = CN_1. \quad (9)$$

To calculate birefringence values at each point of the sheared sample [Fig. 3(c)], a radial distribution of N_1 has to be known. Recently, it was demonstrated that N_1 can be calculated for polymers from an empirical equation:²⁹

$$N_1(\dot{\gamma}) \cong 2\dot{\gamma}\eta \left(1 - \frac{\eta_c^2}{\eta^2}\right)^{0.5} \left(\frac{\eta_c^2}{\eta^2}\right)^{-0.7} \quad (10)$$

where $\dot{\gamma}$ is the shear rate applied to the material, η is the material viscosity ($\eta = \sigma_{12} / \dot{\gamma}$) and η_c is the consistency ($\eta_c = d\sigma_{12} / d\dot{\gamma}$). If shear-rate dependence of the polymer melt viscosity at a required temperature is available [Fig. 4(a)], the two latter parameters can be expressed via Cross model:¹

$$\eta(\dot{\gamma}) = \frac{\eta_0}{1 + (\dot{\gamma} / \dot{\gamma}_c)^m} \quad (11)$$

where the zero shear viscosity η_0 , the critical shear rate $\dot{\gamma}_c$ and the exponent m are rheological parameters of the

polymer melt obtainable from experimental data fitting. Thus, substitution of η and η_c in eq 9 by using eq 10 makes N_1 solely dependent on shear rate [Fig. 4(a)]. The function of radial distribution of shear rates in the rotational plate–plate geometry is known¹

$$\dot{\gamma} = \frac{\Omega r}{d} \quad (12)$$

where Ω is angular speed of the rotating plate and d is the gap between the shearing plates [Fig. 3(b)]. Thus, N_1 can be easily calculated for each point of the sheared sample, thereby allowing calculations of birefringence from eq 9 and, consequently, the phase shift from eq 2. Considering that polarizer and analyzer are crossed at 90°, and that the flow direction is always normal to the radial direction of each point [vector 3, Fig. 3(b)], a PLI of the sheared polymer melt can be calculated from eq 5 [Fig. 4(b–d)]. It was assumed in the calculations that the stress–optical relationship is valid within the range of shear rates used. Considering that the SOC value of LDPE at 150 °C is about $2 \times 10^{-9} \text{ m}^2/\text{N}$ and that in accordance with the theory of ideal rubbers SOC would have only insignificant changes within a relatively narrow temperature interval,¹⁴ it was taken in the PLI calculations that SOC value of LDPE at 125 °C is $2.0 \times 10^{-9} \text{ m}^2/\text{N}$.

The angular speed of the rotating disk controls the range of shear rates applied to the sample. In accordance with the radial distribution of shear rates in plate–plate geometry [Fig. 3(b)], the stress experienced by the polymer melt increases from the center of the sample, where the shear rate is zero, to the edge of the sample with a simultaneous decrease in the stress ellipsoid orientation angle, χ [Fig. 3(b)]. These results in an increase in the aspect ratio of both the indicatrix and its projection onto the 1,3-plane. When the principal directions of the stress ellipsoid form zero angle with the polarizer or analyzer axis, isoclinic fringes (or isogyres) appear in the PLIs, resulting in the extinction pattern similar to Maltese cross [Fig. 4(b)]. The centrosymmetric pattern is formed due to the fact that the stress is radially distributed in the melt subjected to a rotational shear flow. The Maltese cross shape depends on the disk angular speed: the higher the speed the smaller the dark central part of the Maltese cross defined by the four tips moving toward the center of the calculated PLIs [cf., Fig. 4(b,c)]. The position of the features observed in the PLIs corresponds to the same shear rate value, irrespective of the angular speed used for the rotation. Thus, at higher angular speeds, producing a broader range of shear rates along the radius, the Maltese cross pattern observed at a small angular speed [Fig. 4(b)] shrinks and additional black isostress rings, corresponding to the conditions when light intensity is zero, appear [Fig. 4(d)]. The light intensity forms a radial periodic pattern with minima corresponding to $\delta = 2\pi u$, where $u = 0, 1, 2, \dots$ is the order of a minimum. In a case of a white light illumination a periodic pattern of rainbow-like color rings appears.²⁰ This is due to the radial positions of intensity

minima for different wavelengths becoming shifted from each other resulting in isochromatic rings of alternating colors.

Considering the assumptions made in eqs (8–11), a reasonable correlation can be found between the calculated PLI [Fig. 4(b)], based on the viscosity measurements of the LDPE melt, and the actual experimental PLI for the LDPE melt obtained by SIPLI polariscope at flow conditions similar to the calculation [Fig. 4(e)]. This comparison demonstrates that the SIPLI technique has the potential for truly quantitative birefringence measurements. Unfortunately, it was not possible to reproduce experimentally the flow parameters used for the calculations of the other two PLIs [Fig. 4(c,d)] since the normal force generated by the melt at these flow conditions exceeded the rheometer normal force limit (50 N).

A different PLI pattern is obtained for Case (ii), where birefringence changes stepwise along the radius of a sheared sample [Fig. 5(a)]. Contrary to Case (i), the step function is now valid for all wavelengths of the visible spectrum and, therefore, a similar pattern should be expected for both white broadband light and monochromatic light illumination. The expected stepwise change of birefringence is observed for diblock copolymers self-assembling in a lamellar phase [Fig. 5(b)]. It has been shown in a number of theoretical and experimental studies^{22,30,31} that lamellae align parallel to the shear direction at low shear rates (the lamellar normal is parallel to the velocity gradient direction, $\nabla\vec{v}$) and perpendicular to the shear direction at high shear rates (the lamellar normal is parallel to the neutral direction, $\vec{v} \times \nabla\vec{v}$). SIPLI and rheology measurements performed on PS–PI copolymer in acrylate solutions have unambiguously demonstrated that the transition of lamella orientation from parallel to perpendicular occurs at a critical shear rate, $\dot{\gamma}_c$, equal to the inverse relaxation time of the PS–PI chain.²² It has to be noted that a lamellar structure has a uniaxial negative birefringence described by an oblate ellipsoid indicatrix with its minor axis parallel to the lamellar normal.³² Thus, light rays orthogonal to the lamellar planes do not experience birefringence. In analogy to Case (i), a PS–PI sample sheared in rotational plate–plate geometry produces PLIs with an extinction pattern similar to a Maltese cross [Fig. 5(c)]. However, this pattern is composed of two distinctive regions: the non-birefringent (dark) central part of the image of radius r_c corresponding to parallel lamellae and the birefringent (outer) part of the PLI (characterized by a set of four symmetrically disposed sectors of extinction) corresponding to perpendicular lamellae, with their layer normals oriented radially [Fig. 5(b)]. The sharp boundary observed in the PLI between these regions [Fig. 5(c)] corresponds to $\dot{\gamma}_c = 90 \text{ s}^{-1}$ [Fig. 5(a)]. Applying a similar ideology as with the LDPE melt, but using a stepwise function for Δn dependence on shear rate [Fig. 5(a)], the intensity I_{\perp} can be calculated from eq 5 for each point of the sample image. The calculated PLI [Fig. 5(d)] again agrees well with the experimental PLI pattern [Fig. 5(c)].

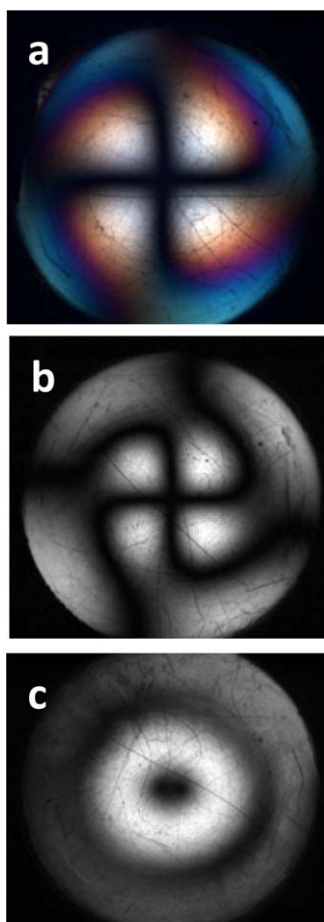


FIGURE 6 Representative PLIs of a LDPE melt taken at the start-up of a shearing pulse during the viscosity overshoot period (temperature 125 °C, angular speed $\Omega = 0.22$ rad/s and $d = 0.7$ mm) using different optical settings (see Fig. 1 for details): (a) a plain reflection polariscope coupled with a white light source (halogen lamp), PLI comprised of isoclinic fringes and isochromatic rings is observed; (b) a plain reflection polariscope coupled with a monochromatic light source (white light filtered by a narrow-band interference filter for wavelength 500 nm), monochromatic PLI comprised of isoclinic fringes and isostress rings is observed; (c) a circular reflection polariscope coupled with a monochromatic light source, monochromatic PLI comprised of isostress rings is observed. The polarizer axis and the analyzer axis are set orthogonal in all three settings. The fast and slow axes of the circular polarizer (the first quarter wave plate) are oriented to the polarizer axis at $\pi/4$ and the fast and slow axes of the circular analyzer (the second quarter wave plate) are crossed to the circular polarizer axes.³³ [Color figure can be viewed in the online issue, which is available at wileyonlinelibrary.com.]

The plain reflection polariscope can be equipped with three more optical components: a narrow-band interference filter and two quarter wave plates (these components are dashed and signed in *italic* in Fig. 1). The filter inserted in the optical path after the white light source allows monochromatic light illumination of a sheared sample. When such a set-up is used, instead of a multicolored PLI comprised of isoclinic

fringes and isochromatic (isostress) rings observed with a white light illumination [Fig. 6(a)] a monochromatic PLI, comprised of isoclinic fringes and isostress rings associated with the selected wavelength of light is obtained [Fig. 6(b)]. Since the latter PLI corresponds to a particular wavelength of light, the intensity of the image points recorded in an experiment can be used for birefringence measurements. Two configurations are commonly used for polariscope studies: a plane polariscope using linear polarized light to produce isostress and isoclinic fringes, and a circular polariscope using circularly polarized light to produce only isostress fringes.³³ An incorporation of two circular polarizers (achromatic quarter wave plates were used in this study) in the optical system (Fig. 1) turns the plain reflection polariscope into a circular reflection polariscope. In this case, the polariscope produces PLI without isoclinic fringes [cf., Fig. 6(b,c)].

Finally, it would be useful to draw an analogy between SIPLI technique and optical methods developed in mineralogy for the crystal birefringence observations. Following the terminology used in microscopy the proposed mechano-optical rheometer exploits an orthoscopic illumination. This means that the sample is viewed perpendicular to the light path and all rays entering the sample and emerging from the sample are parallel (Fig. 1). If a uniaxial single crystal plate of a constant thickness would be loaded between the parallel disks of the rheometer, the ordinary and extraordinary rays emerging from the rheometer would have the same phase difference at each point of the crystal. As a result, the crystal would produce the same interference color at all points of this orthoscopic PLI. However, the situation changes significantly if this crystal is replaced with a sheared viscoelastic liquid such as a polymer melt. The radial distribution of shear rate across the melt in the plate-plate geometry [Fig. 3(b)] creates a radial distribution of normal stress differences. The latter results in a radial distribution of the melt birefringence linked to the normal stress differences via the polymer SOC. Thus, the phase difference between ordinary ray and extraordinary ray of the beam increases radially from the axis of rotation toward the edge of the sample resulting in a PLI formed by rings of alternating interference colors if a broadband white illumination is used [Fig. 6(a)].²⁰ This PLI pattern is similar to the isochromatic rings observed in a conoscopic PLI of a uniaxial crystal plate of a constant thickness.³⁴

EXAMPLES OF APPLICATIONS OF THE MECHANO-OPTICAL RHEOMETER

Five examples are presented in this section to demonstrate different aspects of measurements using the proposed mechano-optical rheometer. The first section reports a transition of orientation in LCs using plate-plate geometry followed by a section on the orientation of diblock copolymer lamellae using cone-and-plate geometry. The next two sections are dedicated to time-resolved measurements of shear-induced crystallization of semi-crystalline polymers (HDPE)

and morphology transitions in thermo-responsive self-assembled diblock copolymers. In the last section, an application of the SIPLI technique for quantitative birefringence measurements is shown using an LDPE melt sheared in plate-plate geometry.

Orientation in Liquid Crystals

It has been reported previously^{35–37} that the transition from parallel to perpendicular orientation of lamellae occurring in smectic-A-like systems, such as smectic A LCs and concentrated lyotropic solutions, has structural analogies with block copolymers. Thus, it is expected that the lamella orientation in LC could be effectively studied by the SIPLI technique as previously used for diblock copolymers²² (Fig. 5). Two types of orientation are commonly observed in LC experiencing shear: lamellae oriented parallel to the shearing surface and lamellae oriented perpendicular to the shearing surface with their layer normal orthogonal to the flow direction. A reasonable qualitative agreement is found between experimental studies^{38–41} and theoretical predictions^{30,35–37} for smectic-A-like systems. The results show that there is a critical shear rate at which the alignment of the lamella phase switches from a parallel to a perpendicular orientation and that the perpendicular lamellae is the preferential alignment state at high shear rates. In this respect, the well-known 8CB compound, existing in crystal, smectic A, nematic and isotropic (liquid) phase, with the smectic A phase stable within a temperature interval from 21.5 °C to 33.5 °C,^{42,43} could be used as a representative example of the smectic A structures.

Indeed, SIPLI measurements of 8CB in smectic A phase revealed PLIs similar to symmetric diblock copolymers²² with a well-defined boundary indicating a transition from non-birefringent central area of the sample to the birefringent outer part exhibiting a Maltese cross pattern [Fig. 7(a)]. The observed boundary is likely to be associated with the critical shear rate at which lamellae change their orientation from a parallel (non-birefringent) alignment to a perpendicular (birefringent) alignment [for a comparison, see Fig. 5(b)]. This boundary corresponds to $\dot{\gamma}_c = 425 \text{ s}^{-1}$, which is similar to the range of values reported for the lamella orientation of 8CB smectic phase using a Couette cell coupled with SAXS technique.⁴³ It was found in this study that within the temperature interval corresponding to the smectic A phase a mixed parallel and perpendicular orientation (named in the cited work as a- and c-orientation, respectively) was observed at shear rates below $\dot{\gamma}_c$ and a perpendicular orientation was observed at shear rates above $\dot{\gamma}_c$.

The dynamics of the lamella orientation transition during a shear experiment can be followed using time-framed PLIs recorded using a CCD camera. It is convenient to display the time-resolved PLIs in a single image using a slicing operation which can be performed using software such as ImageJ.⁴⁴ The images are sliced by a plane orthogonal to the image plane and viewed as a “stack” [Fig. 7(b)]. In this case, all pixels lying on the slicing plane are regrouped in a single pic-

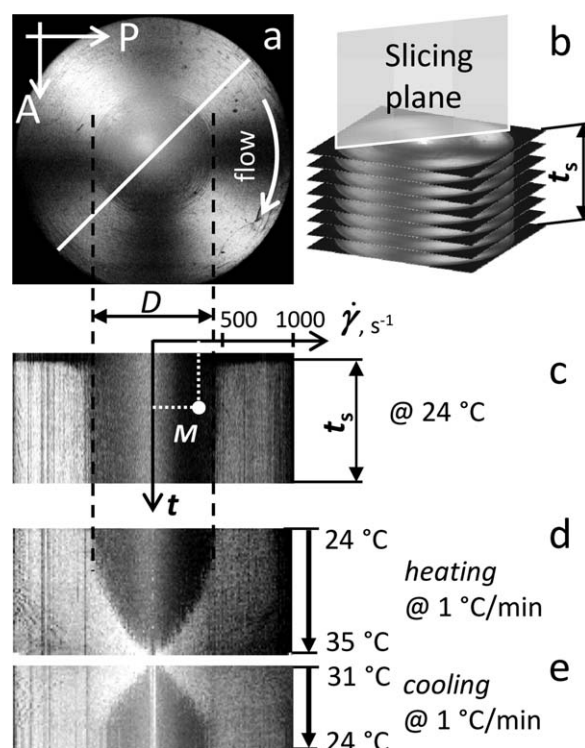


FIGURE 7 SIPLI of 4-*n*-octyl-4'-cyanobiphenyl (8CB) smectic A phase: (a) a representative PLI recorded during a shear pulse at temperature 24 °C (angular speed of rotation of the shearing disk $\Omega = 40 \text{ rad/s}$, gap between the shearing plates $d = 0.5 \text{ mm}$, radius of the sample $R = 12.5 \text{ mm}$ and time of shearing $t_s = 60 \text{ s}$), in the image the shear rate increases radially from 0 s^{-1} at the sample center to $\dot{\gamma}_{\text{max}} = 1000 \text{ s}^{-1}$ at the sample edge ($\dot{\gamma}_{\text{max}} = \Omega R/d$); (b) slicing of the stacked PLIs recorded during this shear pulse and (c) the resulting slice of the PLIs obtained by the slicing plane oriented at 45° to the polarizer and the analyzer; (d) and (e) slices of the PLIs recorded during a shear pulse performed upon heating and cooling, respectively (temperature range from 24 °C to 35 °C covering interval of smectic A phase stability, heating/cooling rate 1 °C/min).

ture representing a cross section (or a slice) of the stacked images. Such a representation of the images enables a process recorded during the experiment (e.g., an evolution of the boundary between the lamella orientations in a sheared sample) to be observed in a single picture. A position of the slicing line in the image depends on analysis requirements. However, slicing performed by a plane forming an angle of 45° with the polarizer/analyzer plane and passing through the axis of rotation [Fig. 7(a,b)] appears to be most efficient. In this case ϕ equals $\pi/4$ for all points of the slice [Fig. 3(a,c)] and, according to eq 5, the intensity contrast between birefringent area and non-birefringent area of the image along this slicing line is maximal. The slice is symmetric with respect to the medium line corresponding to the position of the rheometer rotation axis. Slicing performed in such a way produces a 2D picture of the shear experiment, where coordinates of the points are time and shear rate [Fig. 7(c), see point *M* as an example]. The slice shows that the boundary

of transition between parallel and perpendicular orientation of the smectic lamellae does not change its position with time during the shear pulse. Thus, this result clearly demonstrates that the transition of the lamella orientation is controlled by shear rate which is fully consistent with previous theoretical works indicating that the reorientation of lamellae is a first-order transition occurring at a unique value of the shear rate.^{30,36,37}

It can be demonstrated that the measured $\dot{\gamma}_c$ is a characteristic parameter of the material and is independent of the experimental measurement or setup. In plate-plate geometry, the range of shear rates applied across a sample expands proportionally to the increase in angular speed of the rotating disk, eq 12. Hence, the diameter of the lamella transition boundary [Fig. 7(a)] will be halved upon increase in the angular speed by a factor of two. This is exactly what was observed experimentally (not shown). The boundary moved inwards in a way similar to diblock copolymer lamellae²² retaining its position at $\dot{\gamma}_c$.

SIPLI measurements of the sheared 8CB sample upon heating [Fig. 7(d)] and subsequent cooling [Fig. 7(e)] revealed that $\dot{\gamma}_c$ is temperature dependent. Slices of the PLI stacks demonstrate that the boundary between smectic lamella orientations shifts toward lower values of $\dot{\gamma}$ at high temperatures before reaching 0 s^{-1} at about $34 \text{ }^\circ\text{C}$, being the transition temperature from smectic A phase to the nematic phase [Fig. 7(d)]. A similar thermal dependence of $\dot{\gamma}_c$ has been observed in another work.⁴³ The behavior of the lamella orientation is reversible; the boundary recovers to the original position upon cooling after transition from nematic phase to smectic A phase [Fig. 7(e)]. The presented examples demonstrate that a relatively simple laboratory experiment using a SIPLI polariscope can be effective for quantifying flow parameters responsible for the transition of structural orientations in LCs. Moreover, the technique could be used for time-resolved measurements of the process kinetics and producing the $\dot{\gamma}$ -time [Fig. 7(c)] and/or $\dot{\gamma}$ -temperature [Fig. 7(d,e)] phase diagrams.

Orientation in Block Copolymer Solutions

This section reports about mechano-optical rheological measurements of the lamella orientation in block copolymer solutions using cone-and-plate geometry. This geometry ensures that every point of a sample experiences the same shear rate. Thus, in contrast to the rotational plate-plate geometry [Fig. 3(b)], the lamella orientation of a copolymer solution sheared in cone-and-plate geometry at a particular shear rate has to be radially independent and, therefore, remain the same through the entire sample.

It has to be noted that one of the conditions for the formation of an undistorted PLI is that the surface of the shearing fixture (i.e., the rotating disk) has to be normal to the optical beam (Fig. 1). In this case, all illuminating rays pass the same distance in the sample and, furthermore, both the ray entering the rheometer and the corresponding outgoing (reflected) ray travel via the same path. However, it has been

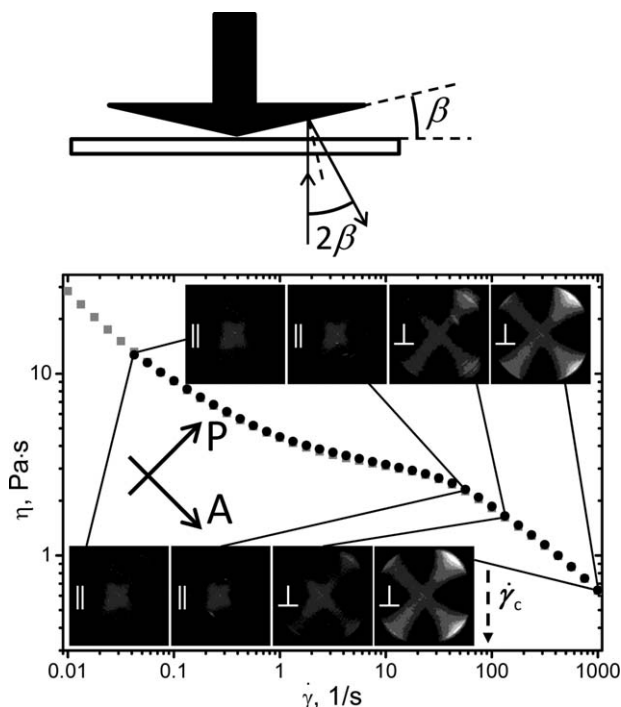


FIGURE 8 A steady-state shear viscosity of 9 wt % acrylate-based solution of polystyrene–polyisoprene (PS–PI) diblock copolymer measured in cone-and-plate geometry (plate diameter 25 mm and cone angle $\beta = 4^\circ$) during ascending and descending shear rate sweeps from 0 s^{-1} to 1000 s^{-1} (circles) and from 1000 s^{-1} to 0 s^{-1} (squares), respectively. The viscosity curves in both cases are virtually identical suggesting reversibility of the structural changes taking place in the material under shear. Representative monochromatic PLIs (wavelength of light is 500 nm) linked to the corresponding viscosity points are shown for both the ascending sweep (the low row of images) and the descending sweep (the top row of images). The dashed vector indicates the critical shear rate value ($\dot{\gamma}_c = 90 \text{ s}^{-1}$) at which the parallel-to-perpendicular orientation transition of the PS–PI lamellar phase occurs (Fig. 5). The measurements were performed at $20 \text{ }^\circ\text{C}$. The top section of the figure schematically shows the path of an optical ray in cone-and-plate geometry.

estimated before using a polymer melt example²⁰ that the deviation of a ray for a few degrees from normality produces insignificant distortions of PLIs. Thus, an optical setup producing small ray deviations can be applied for qualitative PLI observations, which suggests that SIPLI technique could be coupled with cone-and-plate geometry. Indeed, the cone angle β is usually within a range of values between 1° and 4° and a substitution of the top flat shearing disk of the original setup (Fig. 1) by a cone fixture would only cause a small deviation of the outgoing ray from the normal direction of the corresponding entering ray, which is equal to a twofold value of the cone angle (Fig. 8). The gap between shearing surfaces in cone-and-plate geometry is radially dependent as $d = r \tan \beta$. Thus, according to eq 2 the resulting optical retardation is defined by both sample birefringence and the radial position of sample points. This circumstance has to be taken

into account when analyzing PLI data collected using cone-and-plate geometry.

The combination of SIPLI technique with cone-and-plate geometry provides an opportunity to monitor structural properties of a sheared sample during steady-state viscosity measurements. In this respect, ordering of block copolymer microdomains, studied intensively in connection with their rheological⁴⁵ and structural responses,⁴⁶ conveniently suits the proposed SIPLI setup. In particular, a great deal of attention has been paid to the lamellar phase of block copolymers.⁴⁷ It is known that lamellae align parallel (the lamellar normal is parallel to the velocity gradient direction) at low shear rates and perpendicular (the lamellar normal is parallel to the neutral direction) at higher shear rates (Fig. 5). A comparison of independent SIPLI, SAXS, and rheological measurements performed on PS-PI acrylate solutions has demonstrated that the orientation of lamellae changes at a critical shear rate, $\dot{\gamma}_c$, equal to the inverse relaxation time of PS-PI chains.²² The mechano-optical setup proposed in the current work (Fig. 1) enables simultaneous SIPLI and viscosity measurements providing an opportunity for establishing a correlation between the lamellar phase orientation and rheological behavior of the material in a single experiment (Fig. 8). The steady-state viscosity curves measured by the mechano-optical rheometer reproduce previously reported data.²² In the low shear rate region of the plot the viscosity decreases as the shear rate increases. Upon approaching the $\dot{\gamma}_c$ value, when PS-PI lamellae should change their orientation from parallel to perpendicular in plate-plate geometry (Fig. 5), the gradient of the viscosity curve decreases. In the high shear rates region ($\dot{\gamma} > \dot{\gamma}_c$), where perpendicular alignment is expected, thinning becomes pronounced again. This viscosity behavior is consistent with non-equilibrium molecular dynamics simulations, demonstrating that perpendicular lamellae are less viscous than parallel lamellae.³⁶ The viscosity curves measured during ascending and descending of shear rate virtually overlap with each other demonstrating reversibility of the structural changes taking place in the material under the shear flow. At the same time two distinctive groups of PLI patterns are recorded by SIPLI. A clear Maltese cross is observed at high shear rates ($\dot{\gamma} > \dot{\gamma}_c$) indicating that the sheared sample is birefringent (Fig. 8). Indeed, if the PS-PI lamellae are perpendicular, as expected for this range of shear rates, all lamellae in the rotational shearing geometry have to form coaxial rings with their lamella normals (and corresponding n_e axes of the optical indicatrices) oriented radially [see Fig. 5(b) for analogy]. When n_e axes of the coaxial lamellae form a zero angle with the polarizer (or analyzer) axis, isogyres shaped in a Maltese cross appear in the PLIs (Fig. 8). PLIs without Maltese cross, indicating no birefringence, are obtained at low shear rates ($\dot{\gamma} < \dot{\gamma}_c$). These PLI patterns are associated with the parallel orientation of PS-PI lamellae. In this case the lamella normals and n_e axes of the optical indicatrices are parallel to the direction of the entering light beam. Thus, the light wavefront coincides with the circular cross section of the optical indicatrix ellipsoids and the light rays experience n_o

only [as shown in the central part of Fig. 5(b)]. As a result, no birefringence is observed in this case. The optical response of the PS-PI solution registered by SIPLI during shear shows that the transition from parallel alignment to perpendicular alignment occurs close to $\dot{\gamma}_c$. Thus, these data show that the diblock copolymer viscosity changes detected by the mechanical rheology are dictated by the lamella orientation, which is revealed by simultaneous SIPLI measurements.

It has been found that the lamellae can be arrested in parallel or perpendicular orientation by a sudden stop (or a high deceleration rate) of a rotating disk shearing diblock copolymer at $\dot{\gamma} < \dot{\gamma}_c$ or $\dot{\gamma} > \dot{\gamma}_c$ respectively. In this respect SIPLI technique coupled with steady-state rheology can be used to control the pre-orientation of lamellae before and during dynamic rheology measurements of block copolymers in different structural orientation. These results are presented in details elsewhere.²²

Flow-Induced Crystallization of Polymer Melts

The SIPLI technique has already been successfully applied to measure the dynamics of shear-induced crystallization in polymers.¹⁵ Using the effect of birefringence in semi-crystalline polymers, the flow parameters associated with the onset of shear-enhanced nucleation and the shish formation (fibrillation) have been identified (and measured) by SIPLI. In addition to these results, the mechano-optical rheometer proposed in the current work enables optical and rheological measurements to be performed simultaneously. Thus, the observed birefringence phenomena associated with the formation of structural morphologies can be linked to the mechanical properties of a sheared sample. The aim of this section is to demonstrate potential applications of the SIPLI-rheometer setup for studying FIC.

HDPE of an industrial grade was chosen for the measurements. The polymer was loaded onto the rheometer (plate-plate rotational geometry) and after subsequent heating, a shear pulse was applied to the polymer melt. PLIs and the viscosity were recorded during this procedure (Fig. 9). Since the plate-plate geometry is used, the viscosity results obtained during these steady-state measurements can be considered only qualitatively. As discussed in the LC section (Fig. 7), it could be informative presenting the observed PLIs [Fig. 9(a)] as a slice of the collected images [Fig. 9(b)]. The slice conveniently shows the development of sample birefringence during the shear pulse in one picture. Each point of the 2D picture represents the polymer melt response to a particular shear rate for a particular time of shearing.

The PLIs show that the polymer melt is non-birefringent under quiescent conditions prior to the shear pulse [Fig. 9(a), 0 s]. A Maltese cross appears at the beginning of the shear pulse, indicating stress-induced birefringence, and this feature remains in the images throughout the entire time of shearing [Fig. 9(a)]. Under shear the polymer molecules tend to orient along the flow direction and optical indicatrix of the polymer melt turns from sphere to ellipsoid (Fig. 3). Due to the radial distribution of stress in the melt subjected to a

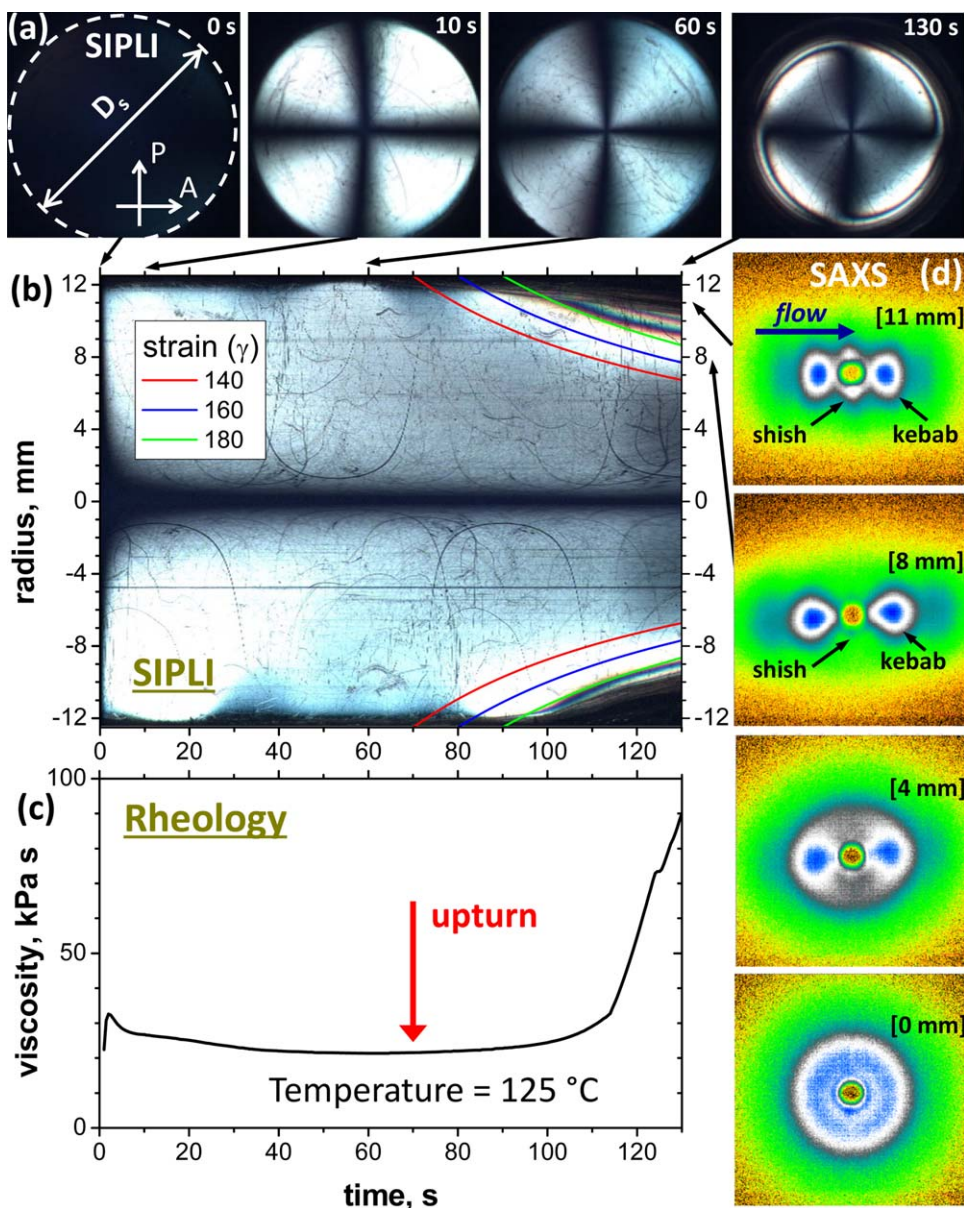


FIGURE 9 (a) Four representative shear-induced PLIs of a polyethylene melt (HDPE, $M_w = 227$ kDa, $M_w/M_n = 14.5$) recorded during a shear pulse ($D_s = 25$ mm, $\Omega = 0.08$ rad/s, $\dot{\gamma}_{\max} = 2$ s $^{-1}$, $d = 0.5$ mm, $t_s = 130$ s, and temperature = 125 °C); the numbers in the right top corner of each image show the time of shearing. (b) A slice of all PLIs stacked together (sliced by a plane oriented at 45° to the polarizer and analyzer plane, see Fig. 7 for further details about the slicing procedure); y-axis shows radial position on the sample and the x-axis is time of shearing; multicolored solid curves show isolines of constant strain. (c) A steady shear viscosity of the HDPE melt measured simultaneously by the rheometer during the shear pulse. (d) Four representative small-angle X-ray scattering (SAXS) patterns of the HDPE sample disk crystallized after the shear pulse, the disk was scanned along the diameter and the patterns correspond to the shish-kebab morphology zone (11 mm from the disk center), the boundary of the shish-kebab zone (8 mm), the oriented shear-enhanced point nuclei zone (4 mm) and the spherulitic zone (0 mm); the side length of the SAXS patterns equals to 0.1 Å $^{-1}$. The SAXS patterns were acquired using a Bruker AXS Nanostar instrument equipped with a 2D HiSTAR multiwired gas detector, modified with a microfocus Xenocs Genix 3D X-ray source (CuK $_{\alpha}$ radiation) and a collimator comprised of motorized scatterless slits, and camera length of 1.46 m. [Color figure can be viewed in the online issue, which is available at wileyonlinelibrary.com.]

rotational shear flow, a Maltese cross is observed in PLIs [Fig. 4(b,c)]. There is a transient increase and decrease in viscosity at the start-up of the shear flow for the first tens of seconds indicating stress “overshoot” [Fig. 9(c)]. This is

reflected in the PLI slice as a bright white area fading out with time at the later shearing stage corresponding to a steady-state regime. If the first normal stress difference is larger than in the experiment presented, a rainbow-like

pattern occurs instead of the bright white area, which would be observed in the PLI slice (see Fig. 5 of ref. 20).

An upturn of viscosity is observed after a continuous shearing for about 70 s [Fig. 9(c)]. It can be noticed in the PLI slice [Fig. 9(b)] that this time coincides with the appearance of a bright white area at the edge of the sample showing a change of birefringence properties of the polymer melt at a point of the highest shear rate ($\dot{\gamma}_{\max}$). The white area transforms into a set of alternating colors at a later stage of the pulse indicating a jump in the melt birefringence, which is potentially associated with the formation of a crystalline morphology. This can be easily observed if one would follow lines of an imaginary grid drawn parallel to the x -axis near the sample edge. Each of these lines corresponds to a radial position on the sample related to a particular shear rate via eq 12. This grid makes it possible to determine that the lower the shear rate the later the birefringence jump appears. This dependence is observed on the PLI slice as a curve formed by alternating colors. In a PLI, the birefringence jump is observed as a circumference between the central dark zone and the bright outer zone [Fig. 9(a), 130 s]. The curve of alternating colors, developing from the zone of high shear rates to the zone of low shear rates, should be associated with the formation of a shish morphology.²¹ Indeed, SAXS measurements, performed on the sample disk crystallized after the shear experiment, confirm this hypothesis [Fig. 9(d)]. Representative SAXS patterns obtained from a radial scan across the sample show that the shish-kebab morphology is observed only within the outer zone of the sample at radii larger than the radial position of the color boundary [Fig. 9(d), 8 mm and 11 mm]. The SAXS patterns demonstrate a clear meridian streak corresponding to a fiber structure (shishes) and two equatorial reflections indicating the formation of oriented lamellar stacks (kebabs) with their layer normals parallel to the flow.^{48,49} At the same time only oriented lamellae associated with shear-enhanced point nuclei [Fig. 9(d), 4 mm] or isotropic spherulites at the center of the sample [Fig. 9(d), 0 mm], and no shish morphology, are observed within the inner zone of the sample. Thus, the color boundary front present in the PLI slice [Fig. 9(b)] indicates the trajectory of flow parameters (shear rate vs. time of shearing) required for the formation of shish structure. As a first approximation, the formation of fibers, or so-called shish morphology, is controlled by shear strain.²¹ The observed curves of alternating colors correlate reasonably well with the isolines of constant strain [Fig. 9(b)]. The isoline corresponding to a shear strain $\gamma = 140$ tracks the edge of the white area associated with the birefringence jump. Since the shearing geometry is fully defined, it is possible to attribute the progression of the boundary of shish formation to a shear rate. Thus, the SIPLI technique enables determination of the flow parameters required for shish formation. The rheology data show that the viscosity upturn begins at 70 s [Fig. 9(c)]. This time corresponds to a strain of 140 at the sample edge ($\dot{\gamma}_{\max} = 2 \text{ s}^{-1}$), where the shish morphology, detected by SIPLI, is initially formed in the sheared sample. Thus, the correlation between SIPLI and rheology data sug-

gests that the viscosity upturn observed during the shear pulse is caused by the formation of the shish morphology.⁵⁰ These results show that time-resolved SIPLI measurements, simultaneously recording information from all points of a sheared sample associated with a range of radially distributed shear rates, can be used as a combinatorial approach for detecting flow conditions for the onset of shish morphology in semi-crystalline polymer melts.

Thermo-Responsive Block Copolymer Micelles

Amphiphilic block copolymers can self-assemble to form various nanostructures if dispersed in a solvent that is selective for one of the blocks.⁵¹ A number of particle morphologies such as spherical micelles, worm-like micelles (often termed worms), and vesicles are commonly found in these systems.⁵² Among these morphologies, the worms' uniaxial anisotropy causes birefringence that is often utilized for structural characterization of their dispersions under shear.^{53,54} In this respect, dispersions of worms are of potential interest for mechano-optical measurements using SIPLI technique. In the present work aqueous dispersions of poly(glycerol monomethacrylate)-block-poly(2-hydroxypropyl methacrylate) (PGMA-PPMA) diblock copolymer worms were selected as a suitable material for such analysis. It has recently been reported that PGMA-PPMA worms form soft free-standing physical hydrogels due to interworm entanglements.⁵⁵ Moreover, these hydrogels demonstrate thermo-reversible degelation which occurs rapidly on cooling below the critical gelation temperature due to a worm-to-sphere transition.

Mechano-optical rheology of a 5 wt % dispersion of PGMA-PPMA worms displays a strong correlation between gel viscosity and morphological transitions (Fig. 10). Under a continuous shear flow performed during a cooling/heating ramp (from 20 °C to 5 °C and then to 35 °C), a number of events can be identified. During the initial stages of shear, a pulse of the apparent viscosity "overshoot" is registered. This sharp increase in viscosity associated with the shear startup persists for a few seconds until the onset of worm micelle orientation, designated by a Maltese cross observed in a PLI (Fig. 10, image a). The Maltese cross appearance in PLIs of sheared worm micelle dispersions is analogous to polymer melts discussed in the previous section. A sharp decrease in viscosity is observed when most micelles of the sample become oriented along the flow direction (indicated by a pronounced Maltese cross in PLI, Fig. 10, image b) before reaching a steady-state regime. The viscosity then remains reasonably constant until cooling is initiated. On close inspection of a PLI corresponding to this stage of the shear experiment (Fig. 10, image b), a dark disk is observed at the center of the sample. Possibly, this is due to the fact that the worm relaxation time (τ) is somewhat faster in comparison to the shear flow rate ($\dot{\gamma} < 1/\tau$) inside the disk area. As a consequence, the worm micelles are not oriented and the dispersion is non-birefringent in this region of the sample. The edge of the disk corresponds to a shear rate of

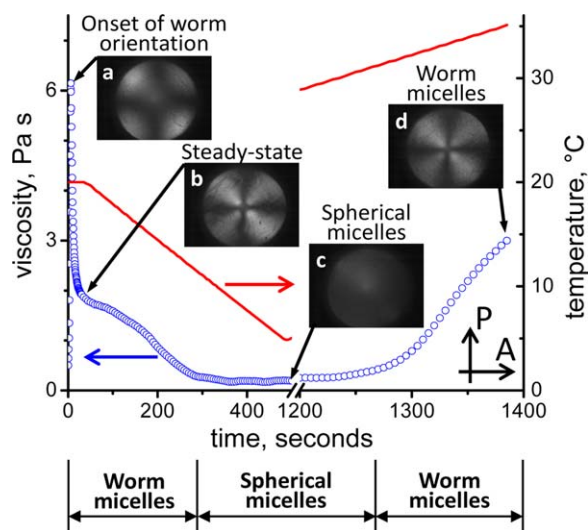


FIGURE 10 Results of mechano-optical rheology of a thermo-responsive PGMA₅₂-PHPMA₁₂₂ diblock copolymer aqueous dispersion (5 wt % solids) obtained during a cooling/heating temperature ramp from 20 °C to 5 °C to 35 °C (plate–plate geometry, $D_s = 25$ mm, $\Omega = 0.08$ rad/s, $d = 1$ mm, and $\dot{\gamma}_{\max} = 1$ s⁻¹). A viscosity plot together with the temperature profile and four representative PLs of the sheared sample corresponding to the onset of worm orientation (a), a steady-state shear regime of the oriented micelles (b), the transformation of worm micelles to spherical micelles upon cooling (c), and the reversible transformation of spherical micelles to worm micelles upon heating (d) are shown. Temperature zones corresponding to the worm micelles and the spherical micelles, defined from both viscosity measurements and SIPLI, are indicated under the plot. The axes of polarizer (P) and analyzer (A) of the SIPLI polariscope are set orthogonal. Pay attention that the time axis of the plot has a breakage after 500 s. [Color figure can be viewed in the online issue, which is available at wileyonlinelibrary.com.]

~ 0.1 s⁻¹, which implies a worm relaxation time of approximately 10 s.

Cooling of the worm dispersion to 5 °C during the shear pulse induces a worm-to-sphere transition,^{23,55} which leads to a loss of the characteristic Maltese cross pattern (Fig. 10, image c). This is due to the isotropic nature of the new species of non-birefringent spherical particles. In addition to the visual observations, the rheometer detects a 10-fold reduction in the dispersion viscosity, as would be expected for such a morphological transformation from entangled worms to non-entangled spheres. On heating, the reverse “sphere-to-worm” transition is observed resulting in both the Maltese cross reappearance (Fig. 10, image d) and viscosity increase. Based on the hysteresis observed during conventional rheological studies,⁵⁵ the dissociative transition upon cooling is expected to be significantly faster than the latter cooperative transition upon heating. Indeed, this pattern of behavior can be recognized from the obtained results: in a comparison with the direct worm-to-sphere transition, a significantly higher temperature and a longer timescale is required to

reform the worms during heating (Fig. 10). The presented example of simultaneous SIPLI and rheology measurements demonstrates the potential of the technique for studying structure–rheological property relationship of worm micelles as well as kinetics of worm transformation under a shear flow.

Birefringence Measurements

The application of SIPLI for qualitative analysis of molecule stretching and structural orientation in soft matter materials as well as quantitative measurements of flow conditions associated with these phenomena have been presented in the four previous sections. Two-dimensional spatial patterns observed in various PLIs were examined and measured in these examples. However, the proposed SIPLI setup can also be used for quantitative measurements of light intensity related to material birefringence via retardation.²⁴ In particular, a plane or circular polariscope consisting of polarizers and quarter-wave plates is adequate for measuring birefringence greater than $10^{-5} - 10^{-4}$.¹⁹ In this respect, the SIPLI polariscope is suitable for studying highly birefringent materials such as polymer melts and solutions.

Before using the mechano-optical rheometer for birefringence measurements, equations necessary for data analysis and some practicalities have to be discussed. Since in the proposed setup an optical beam is normal to the reflecting surface of the shearing disk, measurements of the sample birefringence can be performed in plane defined by axis 1 and axis 3 of the laboratory coordinate (Fig. 3). This birefringence [$\Delta n_{1,3} = n_{11} - n_{33}$, see Fig. 3(b)] is related to a number of parameters measured by a mechanical rheometer. Birefringence can be determined from eq 3 and eq 2 using intensity of light recorded by a camera (Fig. 1). These measurements require monochromatic light illumination, which can be obtained either by inserting an interference filter after the white light source in the optical setup (Fig. 1) or by using a laser coupled with a beam expander. Each 2D intensity pattern (a digital image) recorded during the SIPLI experiment comprises a two-dimensional array of pixels taken at a particular time. The intensity value of each pixel, and its location in the image correspond to a particular area of the studied sample. Thus, the intensity value of an i th pixel of an j th row of the CCD chip, $I(x_i, y_j, t_k)$, contains information about birefringence of the sample at a given point with Cartesian coordinates (x_i, y_j) for a particular time t_k .

The intensity of monochromatic light is usually recorded by a black and white CCD camera as all pixels of the camera are equally sensitive to the incoming signal. However, to keep the original setup, the color CCD camera was adapted for these measurements. The images were recorded in a raw format and to counter the effect of the Bayer filter of the color camera, an extra step was included in the image processing. Half of the image pixels corresponding to red and blue color were excluded from the data analysis and only intensities recorded by the remaining pixels corresponding to green color were used for the birefringence

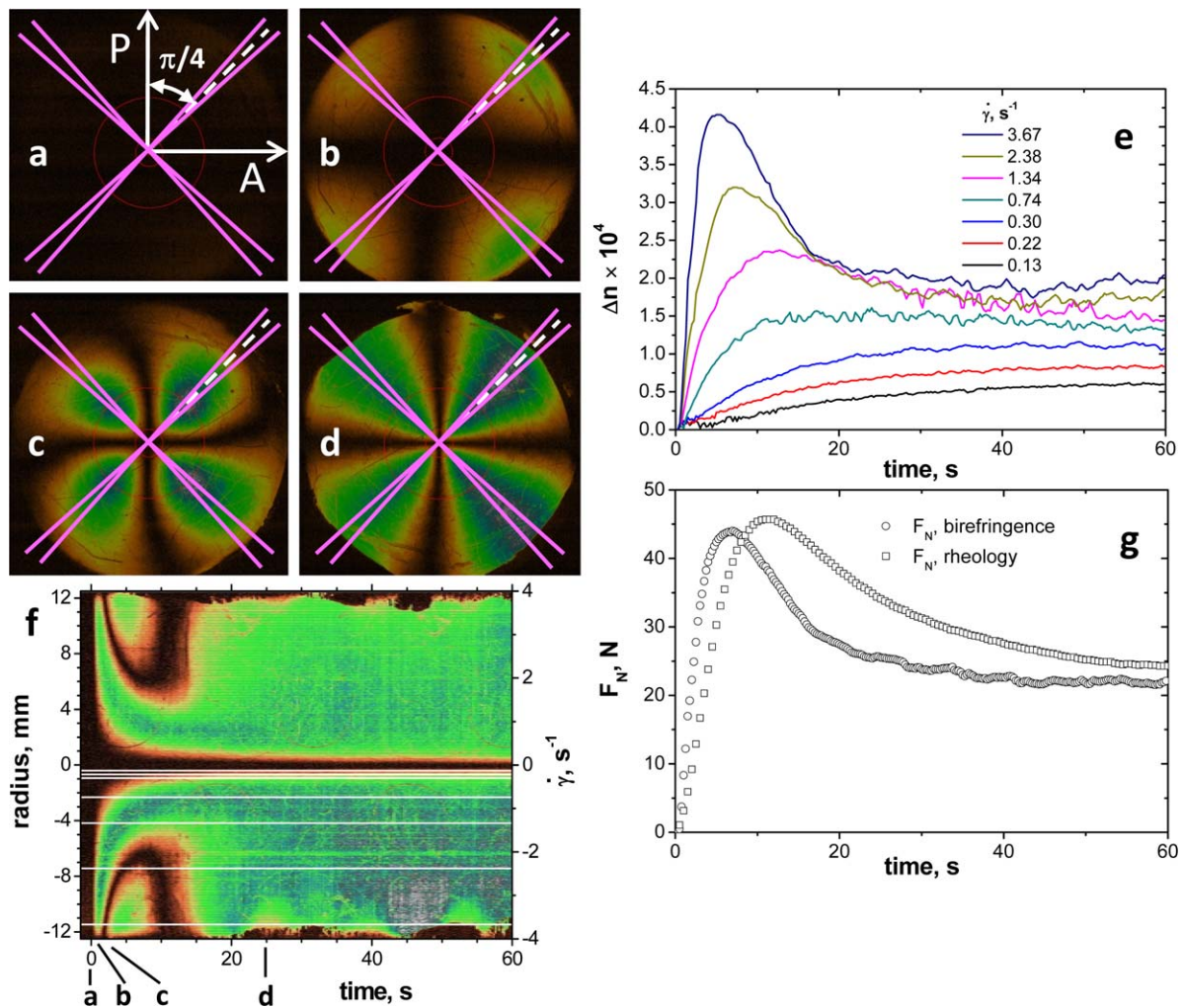


FIGURE 11 An application of SIPLI for birefringence measurements of a sample (LDPE melt at 125 °C) under a shear (plate–plate geometry, $D_s = 25$ mm, $d = 0.7$ mm, $\dot{\gamma}_{\max} = 4$ s⁻¹, $t_s = 60$ s, and wavelength of illuminating light monochromatized by an interference filter, $\lambda = 500$ nm). (a)–(d) Representative pseudo-colored PLIs recorded at different times of the shear pulse: 0 s (a), 1 s (b), 2 s (c), and 25 s (d); the polarizer (P) and analyzer axis (A) are set orthogonal. (e) Time-dependence of the sample birefringence during the shear pulse at different shear rates calculated from the light intensity of PLIs (see text for details). (f) A slice of the stacked PLIs (sliced by a plane oriented in respect to the polarizer axis at 45°, see Fig. 7 and another work²⁰ for the slicing procedure); y-axes show radial position on the sample (left axis) and its corresponding shear rate (right axis); x-axis is time; the white lines parallel to the time axis indicate shear rates for which birefringence curves are presented in section (e) of this figure. (g) A comparison of the normal force values measured by the rheometer transducer during the shear pulse and the total normal force calculated from the birefringence measurements using eq 13, assuming that the second normal stress difference at all points of the sample is zero [$N_2(r) = 0$]. [Color figure can be viewed in the online issue, which is available at wileyonlinelibrary.com.]

calculations. The brightness of the light source was adjusted for avoiding saturation of the pixels during experiments so the registered light signal would be within the camera dynamic range.

Setting up the polarizer and analyzer axis of the instrument mutually perpendicular ($\alpha = \pi/2$) and assuming that the angle of orientation of the optical indicatrix (ϕ) defined by the flow direction is known [Fig. 3(c)], the retardancy of sample points can be calculated from intensity values of the green pixels using eq 5. Subsequently, the birefringence of these points is obtained from eq 2. To demonstrate calcula-

tions of birefringence from monochromatic PLIs, images of an LDPE melt are taken as an example (Fig. 11). It is convenient for the data processing to describe pixel positions in polar coordinates (r_{ij}, ϕ_{ij}) , where $r_{ij} = \sqrt{(x_i - x_0)^2 + (y_j - y_0)^2}$ and $\phi_{ij} = \arctan[|x_i - x_0|/|y_j - y_0|]$. x_i and y_j are relative Cartesian coordinates of a given pixel, and x_0 and y_0 are coordinates of the rheometer rotating axis. Sample points corresponding to positions when maximum intensity of light emerges from the rheometer [$\phi = \pi/4$, eq 6] have been used for the calculations [Fig. 11(a–d)]. Points belonging to four radial directions forming angle ϕ_n with the polarizer axis

($\phi_n = \pi/4 + \pi n/2$, where $n = \overline{0, 3}$) satisfy this condition. Practically, 1D patterns of the radial distribution of intensity along these four directions, $I_{\perp}(r_l, \phi_n, t_k)$, were obtained by an azimuthal integration within sectors of $\pm 3^\circ$ [enclosed by the pink lines in Fig. 11(a-d)], where $l = \overline{0, M}$ is the index of a 1D pattern point and M is a number of points selected along the radial line for integration, $k = \overline{0, N}$ is the image frame index and N is a number of frames recorded during SIPLI experiment. The obtained 1D pattern was subjected to a background subtraction (an image of non-birefringent LDPE melt taken before shearing under quiescent conditions was used as the background). There was no need to perform independent measurements on the incoming light intensity, I_s , as it was possible to determine this value from the recorded PLIs. According to eq 6 $I_{\perp} = I_s$ when $\delta = \pi + 2\pi u$, where $u = 0, 1, 2, \dots$. Thus, I_s can be determined from the intensity of the first interference maximum ($u = 0$) observed in the PLIs [Fig. 11(c), the dark green area in the middle of the four leaves of the 2D pattern]. Considering fourfold symmetry of the PLIs, the intensity is averaged over the four directions, $\overline{I_{\perp}(r_l, t_k)} = \frac{1}{4} \sum_{n=0}^3 I_{\perp}(r_l, \phi_n, t_k) / I_s(\phi_n)$. The product of the data reduction was a two-dimensional $N \times M$ matrix of $\overline{I_{\perp}(r_l, t_k)}$ representing a radial distribution of the normalized averaged intensities for all time frames recorded during the SIPLI experiment. A corresponding $N \times M$ matrix of the retardancy values can be obtained from eq 6:

$$\delta_{lk} = 2 \arcsin \sqrt{\overline{I_{\perp}(r_l, t_k)}}. \quad (13)$$

The retardation increases radially from value of zero at the rotating axis (the sample center) to the maximum value δ_{\max} at the sample edge. When $\delta_{\max} > 2\pi$ the radial distribution of light intensity is a periodic function [e.g., see Fig. 4(d)] and δ_{lk} calculated from $\overline{I_{\perp}(r_l, t_k)}$ should be corrected for its periodicity. Thus, the genuine retardancy values for a particular radial position on the sample are:

$$\begin{aligned} \delta_{lk}^{\text{gen}} &= \delta_{lk} + 2\pi(n-1), \quad r_{\min, n} \leq r_l < r_{\max, n} \\ \delta_{lk}^{\text{gen}} &= -\delta_{lk} + 2\pi n, \quad r_{\max, n} \leq r_l < r_{\min, n+1} \end{aligned} \quad (14)$$

where $r_{\min, n}$ and $r_{\max, n}$ are radial positions of n th minimum and n th maximum of the periodic light intensity values, respectively. For example, $\delta_{lk}^{\text{gen}} = \delta_{lk}$ for $0 \leq r_l < r_{\max, 1}$ and $\delta_{lk}^{\text{gen}} = -\delta_{lk} + 2\pi$ for $r_{\max, 1} \leq r_l < r_{\min, 2}$, where it was assumed that $n = 1$ and $r_{\min, 1} = 0$. The genuine retardancy values can be used further for the calculation of birefringence, $\Delta n_{1,3}$, expressed from eq 2:

$$\Delta n_{1,3}^{lk} = \frac{\delta_{lk}^{\text{gen}} \lambda}{4\pi d}. \quad (15)$$

Each column of the birefringence matrix represents the radial distribution of sample birefringence at a particular time of shearing t_k . Since in rotational plate-plate geometry the radial position of sample points is related to a shear rate (eq 12), each column of the matrix also represents the dependence of sample birefringence on the shear rate. In

this respect, each row of the obtained $\Delta n_{1,3}^{lk}$ matrix represents the development of sample birefringence at a particular shear rate over the time of shearing [Fig. 11(e)]. This development can be represented visually on a pseudo-colored slice of the 2D intensity PLIs [Fig. 11(f)]. The evolution of light intensity with time along each white line shown on the slice corresponds to the birefringence curves plotted in Figure 11(e). For example, the birefringence curve for $\dot{\gamma} = 0.13 \text{ s}^{-1}$ corresponds to the white line nearest to the slice central line where $\dot{\gamma} = 0 \text{ s}^{-1}$. In practice, the slice could be called as a map representing sample birefringence at a given experimental shear rate and time. Thus, the full sample view provided by the SIPLI polariscope allows temporal dependence of material birefringence to be measured simultaneously for a range of shear rates (from 0 s^{-1} to $\dot{\gamma}_{\max}$). The plotted birefringence curves show a transient overshoot at the beginning of the shear pulse before reaching a steady-state regime [Fig. 11(e)]. This behavior is analogous to N_1 of polymer melts measured by mechanical rheology,⁵⁶ which is to be expected since $\Delta n_{1,3}$ is approximately proportional to N_1 (eq 9).

It would be interesting to compare birefringence measured by SIPLI with other parameters recorded simultaneously by the mechanical rheometer during the shear pulse. In this respect, normal force, F_N , is suitable for the comparison. For rotational plate-plate geometry the total F_N on the plate, originating from a sample disk of radius R , is derived by integration as follows:¹

$$F_N = \pi \int_0^R [N_1(r) - N_2(r)] r dr. \quad (16)$$

Assuming that N_2 is close to zero, eq 16 can be rewritten as $F_N = \pi \int_0^R N_1(r) r dr$. Using eq 9, F_N can be approximated via birefringence:

$$F_{N, \text{birefringence}} \approx \frac{\pi}{C} \int_0^R \Delta n_{1,3}(r) r dr. \quad (17)$$

Or, in terms of the carried out SIPLI measurements and analysis, eq 17 can be rewritten in a numerical form:

$$F_{N, \text{birefringence}}(t_k) \approx \frac{\pi}{C} \sum_{l=0}^M \Delta n_{1,3}^{lk} r_l (r_{l+1} - r_l). \quad (18)$$

Thus, using the birefringence matrix calculated from SIPLI data, temporal dependence of the total $F_{N, \text{birefringence}}$ can be obtained from eq 18 and compared with the total $F_{N, \text{rheology}}$ measured in the same experiment by the rheometer transducer [Fig. 11(g)]. In the calculations SOC of LDPE was taken to be $2 \times 10^{-9} \text{ m}^2/\text{N}$.¹⁴ Considering the number of assumptions made in the calculation of $F_{N, \text{birefringence}}$, the F_N curves obtained from the optical and mechanical measurements are reasonably consistent with each other. Some inconsistency between $F_{N, \text{rheology}}$ and $F_{N, \text{birefringence}}$ curves observed during the second half of the shear pulse could be due to the fact that the fracture edge of the sample [(Fig. 11(f)] did not allow reliable birefringence values to be obtained at shear

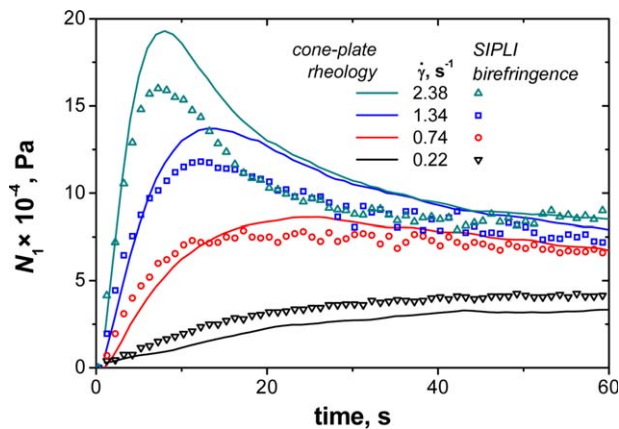


FIGURE 12 The first normal stress difference (N_1) versus time upon start-ups of steady shear of LDPE melt at temperature 125 °C. A comparison of results obtained from optical SIPLI (symbols) and measured by mechanical rheology using cone-and-plate geometry (lines) for four different shear rates is presented; experimental conditions for the SIPLI birefringence measurements: plate–plate geometry, $D_s = 25$ mm, $d = 0.7$ mm, $\dot{\gamma}_{\max} = 4$ s $^{-1}$, $t_s = 60$ s, wavelength of illuminating monochromatic light is 500 nm and experimental conditions for the mechanical rheology: cone-and-plate geometry, cone diameter 12 mm, cone angle 6°, $t_s = 60$ s and $\dot{\gamma} = 0.22$ s $^{-1}$ (black), 0.74 s $^{-1}$ (red), 1.34 s $^{-1}$ (blue), or 2.38 s $^{-1}$ (green). [Color figure can be viewed in the online issue, which is available at wileyonlinelibrary.com.]

rates close to $\dot{\gamma}_{\max}$. Thus, $F_{N,\text{birefringence}}$ obtained from PLIs truncated at high shear rates corresponding to the sample edge should be systematically lower than $F_{N,\text{rheology}}$.

Finally, the birefringence results could be verified by independent rheological measurements. According to eq 9, N_1 can be calculated from SIPLI birefringence:

$$N_1^{lk} \approx \frac{\Delta n_{1,3}^{lk}}{C}. \quad (19)$$

This enables SIPLI data [Fig. 11(e)] to be presented in terms of the normal stress difference (Fig. 12, symbols). At the same time N_1 can be measured for this set of shear rates by a rheometer using cone and plate geometry (Fig. 12, lines). To avoid the influence of a cross flow retardation on the true normal force reading during measurements of highly viscous and elastic LDPE melt,⁵⁶ a cone of a small diameter (12 mm) with a relatively large cone angle (6°) was used for the measurements. Both sets of N_1 data obtained from the SIPLI birefringence and independent mechanical measurements exhibit a similar type of behavior and are consistent with each other (Fig. 12). Some deviations between measured values are observed at higher shear rates during the overshoot stage, after the inception of flow. However, both sets of results agree well quantitatively at the steady-state regime when the N_1 curves level off. It is worth emphasizing that the SIPLI results for different shear rates were obtained simultaneously in one experiment, whereas to collect the mechanical rheology data four independent measurements were required.

CONCLUSIONS

A new method for mechano-optical rheology which combines optical SIPLI and rotational plate–plate (or cone-and-plate) mechanical rheometer has been developed. The method makes it possible to perform simultaneous measurements of both the rheology and birefringence properties of polymeric and soft matter materials. Moreover, these measurements can be carried out over a wide temperature range (from –40 °C to 200 °C). The instrument optical setup is flexible; various combinations of linear and circular polarizers enable full sample view monitoring, time-resolved PLI recordings and quantitative birefringence measurements.

A variant of SIPLI using plate–plate geometry has the advantage of producing a range of shear rates radially distributed across a sheared sample. Since the information is recorded for all parts of the sample experiencing different flow conditions simultaneously, the method can be classified as a combinatorial approach. In this respect the plate–plate geometry can be used to establish relationship between flow parameters and flow-induced phenomena affecting birefringence of soft matter materials in a single experiment. In contrast to the rotational plate–plate geometry, samples sheared in cone-and-plate geometry experience a shear rate which is constant through the entire sample. Thus, a variant of SIPLI coupled with cone-and-plate geometry provides a unique opportunity to monitor sample state during rheological measurements involving continuous shear. It has to be noted that one of the shearing surfaces in this geometry is not normal to the entering optical beam. This makes cone-and-plate geometry less suitable for quantitative SIPLI birefringence measurements.

It is demonstrated that the radial distribution of shear rate in rotational plate–plate geometry can be effectively used for combinatorial studies of flow effects on crystallization of polymer melts, molecular orientation and structural morphology of polymeric and other liquids. A good correlation between experimental and calculated PLI patterns has been found for flow-induced phenomena exhibiting either continuous or step-wise shear rate dependence of material birefringence.

The performance of the method is tested by studying orientation of the lamellar phase in block copolymers and smectic A LCs, shear-induced crystallization of semi-crystalline polymers and morphological transformations of aqueous block copolymer dispersions. The obtained data are consistent with published results measured by other techniques. In particular, mechano-optical rheology revealed that the orientation of the lamellar phase of 8CB and PS–PI diblock copolymer is controlled by shear rate and critical flow parameters of the transition from parallel to perpendicular orientation of lamellae have been measured. A shear rate-temperature phase diagram of the transition of lamella orientation was obtained for 8CB smectic A phase in a single experiment. Simultaneous SIPLI and rheology measurements of PS–PI using cone-and-plate geometry showed that the technique is effective for establishing a relationship between

structural orientation and viscosity. In another example, the birefringence of high-density polyethylene crystals is used to detect the flow parameters associated with the onset of shish formation in a sheared polymer melt and a relationship between the shish formation, detected by SIPLI, and the viscosity upturn, measured by the rheometer at the same time, has been established. Similarly, a mechano-optical rheology of thermo-responsive block copolymer aqueous dispersions revealed a direct relationship between the transition of block copolymer morphology from worm-like micelles to spherical micelles, detected by SIPLI, and the viscosity decrease, measured by the rheometer.

In addition, application of the SIPLI polariscope for quantitative birefringence measurements is demonstrated. Since stress is radially distributed in the rotational plate–plate geometry, both its magnitude and the birefringence produced are constant at all points of the specified circumference. It is found that the normal stress difference values across a sheared polymer melt (LDPE in plate–plate geometry) calculated from the birefringence correlate reasonably well with both the total normal force values measured by the rheometer transducer during the same experiment and the first normal stress differences measured independently on the same polymer using cone-and-plate geometry.

This technique has great potential to go beyond the examples highlighted in this current work. The proposed mechano-optical rheology method is based on shearing material using a geometry with a well-defined range of shear rates, and monitoring the optical response of the sheared material to the effects of this shear. This general approach can be applied to the study of various shear-induced phenomena in complex fluids.

ACKNOWLEDGMENTS

Iakovos Vittorias of Lyondellbasell is thanked for the kind donation of the polyethylene samples used in this work. The authors would also like to acknowledge helpful discussions with Alexei Likhtman on the rheology data. N.J.W thanks EPSRC for a support (EP/J007846/1).

REFERENCES AND NOTES

- 1 C. W. Macosko. *Rheology: Principles, Measurements, and Applications*; VCH Publishers, Inc.: New York, **1994**.
- 2 H. A. Barnes, D. Bell. *Korea-Aust. Rheol. J.* **2003**, *15*, 187–196.
- 3 K. P. Menard. *Dynamic Mechanical Analysis: A Practical Introduction*; CRC Press LLC: Boca Raton, **1999**.
- 4 M. L. Sentmanat. *Rheol. Acta* **2004**, *43*, 657–669.
- 5 M. Boulet-Audet, A. E. Terry, F. Vollrath, C. Holland. *Acta Biomater.* **2014**, *10*, 776–784.
- 6 M. C. Chevrel, S. Hoppe, L. Falk, B. Nadege, D. Chapron, P. Bourson, A. Durand. *Ind. Eng. Chem. Res.* **2012**, *51*, 16151–16156.
- 7 A. I. Nakatani, D. A. Waldow, C. C. Han. *Rev. Sci. Instrum.* **1992**, *63*, 3590–3598.

- 8 J. Lauger, W. Gronski. *Rheol. Acta* **1995**, *34*, 70–79.
- 9 F. Camerel, J. C. P. Gabriel, P. Batail, P. Panine, P. Davidson. *Langmuir* **2003**, *19*, 10028–10035.
- 10 J. P. de Silva, D. Petermann, B. Kasmi, M. Imperor-Clerc, P. Davidson, B. Pansu, F. Meneau, J. Perez, E. Paineau, I. Bihannic, L. J. Michot, C. Baravian. *J. Phys.: Conf. Ser.* **2010**, *247*, 012052.
- 11 B. Struth, K. Hyun, E. Kats, T. Meins, M. Walther, M. Wilhelm, G. Gruebel. *Langmuir* **2011**, *27*, 2880–2887.
- 12 J. Stellbrink, B. Lonetti, G. Rother, L. Willner, D. Richter. *J. Phys.-Condens. Matter* **2008**, *20*, 404206.
- 13 G. G. Fuller. *Optical Rheometry of Complex Fluids*; Oxford University Press: Oxford, **1995**.
- 14 H. Janeschitz-Kriegl. *Polymer melt rheology and flow birefringence*; Springer-Verlag: Berlin, **1983**.
- 15 F. D. Dexter, J. C. Miller, W. Philippoff. *Trans. Soc. Rheol.* **1961**, *5*, 193–204.
- 16 J. L. S. Wales, H. Janeschitz-Kriegl. *J. Polym. Sci. Part A-2: Polym. Phys.* **1967**, *5*, 781–790.
- 17 M. R. Mackley, D. G. Hassell. *J. Non-Newton. Fluid Mech.* **2011**, *166*, 421–456.
- 18 K. Lee, M. R. Mackley, T. C. B. McLeish, T. M. Nicholson, O. G. Harlen. *J. Rheol.* **2001**, *45*, 1261–1277.
- 19 M. E. Mackay, D. V. Boger. In *Rheological Measurement*; A. A. Collyer, D. W. Clegg, Eds.; Chapman & Hall: London, **1998**, pp 595–634.
- 20 O. O. Mykhaylyk. *Soft Matter* **2010**, *6*, 4430–4440.
- 21 C. Holland, F. Vollrath, A. J. Ryan, O. O. Mykhaylyk. *Adv. Mater* **2012**, *24*, 105–109.
- 22 O. O. Mykhaylyk, A. J. Parnell, A. Pryke, J. P. A. Fairclough. *Macromolecules* **2012**, *45*, 5260–5272.
- 23 A. Blanz, R. Verber, O. O. Mykhaylyk, A. J. Ryan, J. Z. Heath, C. W. I. Douglas, S. P. Armes. *J. Am. Chem. Soc.* **2012**, *134*, 9741–9748.
- 24 M. Born, E. Wolf. *Principles of Optics: Electromagnetic Theory of Propagation, Interference and Diffraction of Light*; Cambridge University Press: Cambridge, **1999**; pp 790–852.
- 25 W. Philippoff. *Trans Soc. Rheol.* **1961**, *5*, 163–191.
- 26 F. H. Gortemaker, M. G. Hansen, B. D. Cindio, H. Janeschitz-Kriegl. *Rheol. Acta* **1976**, *15*, 242–255.
- 27 W. Philippoff. *Rheol. Acta* **1973**, *12*, 425–429.
- 28 J. L. S. Wales, W. Philippoff. *Rheol. Acta* **1973**, *12*, 25–34.
- 29 V. Sharma, G. H. McKinley. *Rheol. Acta* **2012**, *51*, 487–495.
- 30 G. H. Frederickson. *J. Rheol.* **1994**, *38*, 1045–1067.
- 31 H. Leist, K. Geiger, U. Wiesner. *Macromolecules* **1999**, *32*, 1315–1317.
- 32 W. Thornburg. *J. Biophys. Biochem. Cytol.* **1957**, *3*, 413–419.
- 33 R. S. Sirohi. *Optical Methods of Measurement: Wholefield Techniques*; CRC Press: New York, **2009**; pp 201–237.
- 34 F. D. Bloss. *Optical Crystallography*; Mineralogical Society of America: Washington, DC, **1999**.
- 35 G. K. Auernhammer, H. R. Brand, H. Pleiner. *Phys. Rev. E* **2002**, *66*, 061707.
- 36 H. X. Guo. *J. Chem. Phys.* **2006**, *124*, 054902.
- 37 M. Lisal, J. K. Brennan. *Langmuir* **2007**, *23*, 4809–4818.
- 38 J. Penfold, E. Staples, A. K. Lodhi, I. Tucker, G. J. T. Tiddy. *J. Phys. Chem. B* **1997**, *101*, 66–72.
- 39 C. R. Safinya, E. B. Sirota, R. F. Bruinsma, C. Jeppesen, R. J. Plano, L. J. Wenzel. *Science* **1993**, *261*, 588–591.

- 40** J. Zipfel, J. Berghausen, P. Lindner, W. Richtering. *J. Phys. Chem. B* **1999**, *103*, 2841–2849.
- 41** K. I. Winey, S. S. Patel, R. G. Larson, H. Watanabe. *Macromolecules* **1993**, *26*, 2542–2549.
- 42** Y. Ouchi, Y. Takamishi, H. Takezoe, A. Fukuda. *Jpn. J. Appl. Phys. Part 1-Regular Pap. Short Notes Rev. Pap.* **1989**, *28*, 2547–2551.
- 43** C. R. Safinya, E. B. Sirota, R. J. Plano. *Phys. Rev. Lett.* **1991**, *66*, 1986–1989.
- 44** W. Rasband ImageJ V1.45s, **2011**. <https://imagej.nih.gov/ij/>.
- 45** H. Watanabe. In *Structure and Properties of Multi-Phase Polymeric Materials*; T. Araki, Q. Tran-Cong, M. Shibayama, Eds.; Marcel Dekker: New York, **1998**, pp 317–360.
- 46** I. W. Hamley. *Curr. Opin. Colloid Interface Sci.* **2000**, *5*, 342–350.
- 47** S. Sakurai. *Polymer* **2008**, *49*, 2781–2796.
- 48** J. K. Keum, F. Zuo, B. S. Hsiao. *Macromolecules* **2008**, *41*, 4766–4776.
- 49** G. Kumaraswamy, R. K. Verma, J. A. Kornfield, F. J. Yeh, B. S. Hsiao. *Macromolecules* **2004**, *37*, 9005–9017.
- 50** L. Balzano, N. Kukalyekar, S. Rastogi, G. W. M. Peters, J. C. Chadwick. *Phys. Rev. Lett.* **2008**, *100*, 048302.
- 51** L. F. Zhang, A. Eisenberg. *Science* **1995**, *268*, 1728–1731.
- 52** N. J. Warren, S. P. Armes. *J. Am. Chem. Soc.* **2014**, *136*, 10174–10185.
- 53** B. D. Frounfelder, G. C. Kalur, B. H. Cipriano, D. Danino, S. R. Raghavan. *Langmuir* **2009**, *25*, 167–172.
- 54** E. Cappelaere, J. F. Berret, J. P. Decruppe, R. Cressely, P. Lindner. *Phys. Rev. E* **1997**, *56*, 1869–1878.
- 55** R. Verber, A. Blanazs, S. P. Armes. *Soft Matter* **2012**, *8*, 9915–9922.
- 56** J. Meissner. *J. Appl. Polym. Sci.* **1972**, *16*, 2877–2899.